GIScience & Remote Sensing

ISSN: 1548-1603 (Print) 1943-7226 (Online) Journal homepage: www.tandfonline.com/journals/tgrs20

An extensive validation of ocean color products for the black sea

Dalin Jiang, Luis González Vilas , Elizabeth C. Atwood , Vittorio E. Brando , Simone Colella , Violeta Slabakova , Ivelin Petkov , Adriana Maria Constantinescu , Iulian Pojar , Adrian Stanica , Conor McGlinchey , Ximena Aguilar Vega , Douglas Moore , Evangelos Spyrakos & Andrew Tyler

To cite this article: Dalin Jiang, Luis González Vilas , Elizabeth C. Atwood , Vittorio E. Brando , Simone Colella , Violeta Slabakova , Ivelin Petkov , Adriana Maria Constantinescu , Iulian Pojar , Adrian Stanica , Conor McGlinchey , Ximena Aguilar Vega , Douglas Moore , Evangelos Spyrakos & Andrew Tyler (2026) An extensive validation of ocean color products for the black sea, GIScience & Remote Sensing, 63:1, 2662816, DOI: 10.1080/15481603.2026.2662816

To link to this article: https://doi.org/10.1080/15481603.2026.2662816

Published online: 06 May 2026.

GISCIENCE & REMOTE SENSING
2026, VOL. 63, NO. 1, 2662816
https://doi.org/10.1080/15481603.2026.2662816

Taylor & Francis
by informa

RESEARCH ARTICLE

OPEN ACCESS Check for updates

An extensive validation of ocean color products for the black sea

Dalin Jiang[a], Luis González Vilas[b,c], Elizabeth C. Atwood[d], Vittorio E. Brando[b], Simone Colella[b], Violeta Slabakova[e], Ivelin Petkov[e], Adriana Maria Constantinescu[f], Iulian Pojar[f], Adrian Stanica[f], Conor McGlinchey[a], Ximena Aguilar Vega[a], Douglas Moore[a], Evangelos Spyrakos[a] and Andrew Tyler[a]

[a]Earth and Planetary Observation Sciences (EPOS), Biological and Environmental Sciences, Faculty of Natural Sciences, University of Stirling, Stirling, United Kingdom; [b]CNR-ISMAR, Istituto di Scienze Marine, Consiglio Nazionale delle Ricerche, Rome, Italy; [c]Nologin Oceanic Weather Systems (NOW Systems), Santiago de Compostela, Spain; [d]Marine Processes and Observations, Plymouth Marine Laboratory, Plymouth, United Kingdom; [e]Institute of Oceanology, Bulgarian Academy of Sciences (IO-BAS), Varna, Bulgaria; [f]National Institute of Marine Geology and Geo-ecology (GeoEcoMar), Bucharest, Romania

ABSTRACT

Ocean color remote sensing provides an efficient approach to monitor the state and changes in water bodies on Earth. The validation of an ocean color product is a key step in assessing its accuracy, directly influencing the confidence with which conclusions can be drawn. In this study, we compiled a comprehensive *in situ* optical and biogeochemical dataset to assess the performance of ocean color products provided by the Copernicus Marine Service (CMEMS), Copernicus Evolution – Research for harmonized and Transitional water Observation (CERTO), as well as products distributed by the European Organization for the Exploitation of Meteorological Satellites (EUMETSAT) in the Black Sea. Results showed that both the CMEMS and CERTO provide accurate remote sensing reflectance in the Black Sea at visible bands with the highest accuracy at 555 nm or 560 nm, reaching a mean absolute percentage deviation (MAPD) lower than 14%, but higher errors were found in the short-blue (<440 nm) and near-infrared (>700 nm) bands. Chlorophyll-a concentration (Chl-a) products derived from two CMEMS datasets: multi-sensor (CMEMS MULTI) and Sentinel-3 OLCI (CMEMS OLCI), and two CERTO datasets: Sentinel-3 OLCI (CERTO OLCI) and Sentinel-2 MSI (CERTO MSI), agreed with *in situ*-measured values. However, the Chl-a products from EUMETSAT showed larger errors, with MAPDs higher than 150%. The total suspended matter (TSM) concentration products from the EUMETSAT OLCI, CERTO OLCI and CERTO MSI showed good agreements with the *in situ* data. The two diffuse attenuation coefficients for downwelling irradiance at 490 nm ($K_d(490)$) products from CMEMS showed a good accuracy with MAPDs lower than 20%. Recommendations based on the results are provided to further improve the ocean color products in the region, including merging ocean color algorithms developed from different services based on optical water type classifications.

ARTICLE HISTORY
Received 28 October 2025
Accepted 16 April 2026

KEYWORDS
Water quality; ocean color; black sea; earth observation

1. Introduction

About 71% of our Earth is covered by water, of which about 97% are oceanic waters (Douville et al. 2021). The oceans play a crucial role in global hydrological, carbon and nutrients cycles, providing essential ecosystem services, including food, energy, transportation, and recreation, which are closely linked to human well-being (Barbier 2017; Liquete et al. 2013). Monitoring the status and changes of marine and coastal waters are fundamentally important for maintaining their ecosystem functions, especially in the context of global warming, population increasing, and anthropogenic activity intensifying (Aronson et al. 2011; Douville et al. 2021; Duarte 2014). However, routine surveys are unable to cover the scales required to deliver ocean system understanding. Ocean color remote sensing thus provides great benefits in global ocean and coastal water monitoring, as proven since the first ocean color sensor was launched in 1978 (Groom et al. 2019).

CONTACT Dalin Jiang dalin.jiang@stir.ac.uk

The advantages of large spatial coverage and short revisit period of the state-of-the-art satellite remote sensing have allowed them to be widely applied in regional to global scale aquatic environment monitoring (Stramski, Joshi, and Reynolds 2022; Wang et al. 2020; Wilson et al. 2025). Numerous algorithms have been developed for monitoring biogeochemical parameters, including chlorophyll-a concentration (Chl-a, e.g. Hu and Lee, 2012; O'Reilly and Werdell 2019), total suspended matter concentration (TSM, e.g. Jiang et al. 2023; Nechad, Ruddick, and Park 2010), water transparency (e.g. Jiang et al. 2019; Lee et al. 2015), and colored dissolved organic matter (CDOM, e.g. Aurin, Mannino, and Lary 2018; Shanmugam 2011). In addition, platforms providing open access ocean color products support Earth and ocean system research, marine management and policy development. The Ocean Color Thematic Assembly Center (OCTAC) of the Copernicus Marine Service (CMEMS) from the European Union delivers merged ocean color products for the global ocean and European Seas both in near-real time (NRT) and as reprocessed multi-year datasets. In ocean color product development, one of the key steps is the validation of the ocean color algorithm using *in situ* reference data. Although most generated products have been validated during algorithm development stages using *in situ* data, it is always valuable to revisit the developed algorithms and further validate them using newly collected data, covering more regions with wider bio-optical properties.

The Black Sea, located between Asia and Europe, is an enclosed sea connected with the Mediterranean Sea through the Bosporus and provides important ecosystem services for nearby countries (Jiang et al. 2025a; Vespremeanu and Golumbeanu 2017). However, owing to industry expansion, urbanization and agricultural intensification in the catchment, numerous pollutants are discharged into this system through main rivers such as the Danube, Dniester, Dnieper and Bug (Vespremeanu and Golumbeanu 2017). These nutrients have led to eutrophication with severe algal blooms and associated hypoxia area expansion, which compounded with the invasion of alien species and overfishing, led to the Black Sea ecosystem being largely devasted in the 1980s and 1990s (Kideys 2002). The enclosed sea has a long water residence time (on the scale of hundreds of years, Murray, Top, and Özsoy 1991; Wegwerth et al. 2021), making it extremely vulnerable to human activities and slow to recover from pollution (Jiang et al. 2025b). Regular monitoring of this system thus is crucially important for supporting environmental management, protection and restoration. Although many studies conducted in the Black Sea have employed Earth observation focusing on Chl-a (e.g. Barale et al. 2002; Grégoire et al. 2023; Sancak et al. 2005; Suslin and Churilova 2016; Vostokov, Vostokova, and Vazyulya 2022) and TSM or turbidity (e.g. Constantin et al. 2024; Constantin, Doxaran, and Constantinescu 2016; Güttler, Niculescu, and Gohin 2013; Kukushkin and Suslin 2020; Nazirova et al. 2021), most either only focused on parts of the Black Sea or haven't been implemented into services providing routine monitoring with regular updates. The CMEMS, Copernicus Evolution–Research for harmonized and Transitional Water Observation (CERTO), and European Organization for the Exploitation of Meteorological Satellites (EUMETSAT) have developed algorithms specifically including the Black Sea environment (Atwood et al. 2024; Kajiyama, D'Alimonte, and Zibordi 2018) and regularly update ocean color products in the Black Sea with higher spatial resolutions (20–300 m) than other services, such as the European Space Agency Ocean Color Climate Change Initiative (ESA OC_CCI, 4 km). Although efforts have been made for validation of these products using limited *in situ* data during algorithm development stages, the accuracy of these products has not been extensively validated.

This research aims to validate existing ocean color products from CMEMS, CERTO, and EUMETSAT using extensive *in situ* data collected from the Black Sea, and provide recommendations on the improvement of these services and support Black Sea stakeholders, based on the results and findings.

2. Methodology

2.1. In situ data measurements

In situ data were compiled from five main resources: Constantinescu (2019), CERTO project, Horizon 2020 Developing Optimal and Open Research Support for the Black Sea (DOORS) project, bio-optical datasets collected by the Institute of Oceanology-Bulgaria Academy of Science (IO-BAS) within several national and international scientific initiatives, and the Aerosol Robotic Network-Ocean Color (AERONET-OC) platforms. *In situ* remote sensing reflectance (R_{rs}), Chl-a and TSM data from Constantinescu (2019) were collected through two research cruises in the Danube Delta onboard the research vessel (RV) Istros and the

Table 1. Summary of the *in situ* data collected for ocean color validation in this study.

Source	Variable	Time	Location
Constantinescu (2019)	• R_{rs} ($N = 70$) • Chl-a ($N = 99$) • TSM ($N = 101$)	July 2015—May 2016	Danube Delta, Razelm–Sinoe Lagoon
CERTO	• R_{rs} ($N = 20$) • Chl-a ($N = 142$) • TSM ($N = 142$)	April 2021—August 2022	Western Black Sea, Danube Delta, Razelm–Sinoe Lagoon
DOORS	• R_{rs} ($N = 92$) • Chl-a ($N = 94$) • TSM ($N = 92$)	May 2023—June 2024	Western, central, and eastern Black Sea
IO-BAS	• $K_d(490)$ ($N = 36$) • R_{rs} ($N = 182$) • Chl-a ($N = 424$)	July 2011—June 2021	Western and central Black Sea
AERONET-OC	• $K_d(490)$ ($N = 181$) • R_{rs} ($N = 2893$)	Galata: April 2014—December 2023 Gloria: January 2011—August 2019 Section-7: August 2019—August 2024	Western Black Sea

EuroFleets 2 ReCoReD research cruise onboard the RV Mare Nigrum between 2015 and 2016. During CERTO, *in situ* R_{rs}, Chl-a and TSM data were collected between 2021 and 2022 from the Danube Delta and Razelm–Sinoe Lagoon in Romania. During DOORS, data of *in situ* R_{rs}, Chl-a, TSM and diffuse attenuation coefficient for downwelling irradiance at 490 nm ($K_d(490)$) were collected from three dedicated campaigns between 2023 and 2024 covering the western, central and eastern Black Seas. As part of the IO-BAS national monitoring program, *in situ* R_{rs}, Chl-a and $K_d(490)$ data were collected from western and central Black Sea waters between 2011 and 2021. Additionally, *in situ* R_{rs} recorded at three AERONET-OC sites in the western Black Sea (namely, the Gloria, Galata, and Section-7 platforms) between 2011 and 2024 were compiled. A summary of all *in situ* data is provided in Table 1. Locations of the three AERONET-OC sites and the *in situ* measurements from Constantinescu (2019), CERTO, DOORS, and IO-BAS campaigns are shown in Figure 1.

Water samples were collected from the water surface in the field and filtered through 0.7 µm pore size GF/F filters. To measure Chl-a concentration, high-performance liquid chromatography (HPLC) was used for samples collected during the first and second DOORS cruises ($N = 65$), and spectrophotometry was used for the remainder of the samples (Jeffrey and Humphrey 1975). TSM was measured following the gravimetric method. Details of the protocol used for measuring Chl-a and TSM can be found in Jiang et al. (2021a).

R_{rs} measurements were obtained from three shipborne platforms, i.e. Satlantic Micro profiler, HyperSAS and TriOS, and were also available from the three AERONET-OC platforms in the Black Sea. The Satlantic Micro Profiler is a free-fall profiling system (hereafter named Profiler), which simultaneously measures the upwelling radiance $L_u^{0-}(z, \lambda)$ and downwelling irradiance $E_d^{0-}(z, \lambda)$ at multiple bands (412 nm, 443 nm, 490 nm, 510 nm, 555 nm, 665 nm, and 683 nm) from different depths (z) of the water column. R_{rs} were determined from $L_u^{0-}(z, \lambda)$ and $E_d^{0-}(z, \lambda)$ following the protocol by Zibordi et al. (2011). The HyperSAS and TriOS systems measure hyperspectral data between 350 nm and 950 nm with the above-water approach, both of them include three sensors for measuring the total radiance from water (L_t), the sky radiance (L_{sky}), and the downwelling irradiance above the water surface (E_d^{0+}). R_{rs} were then calculated from L_t, L_{sky}, and E_d^{0+}. A further correction for residual reflected skylight for R_{rs} measured using HyperSAS and TriOS was

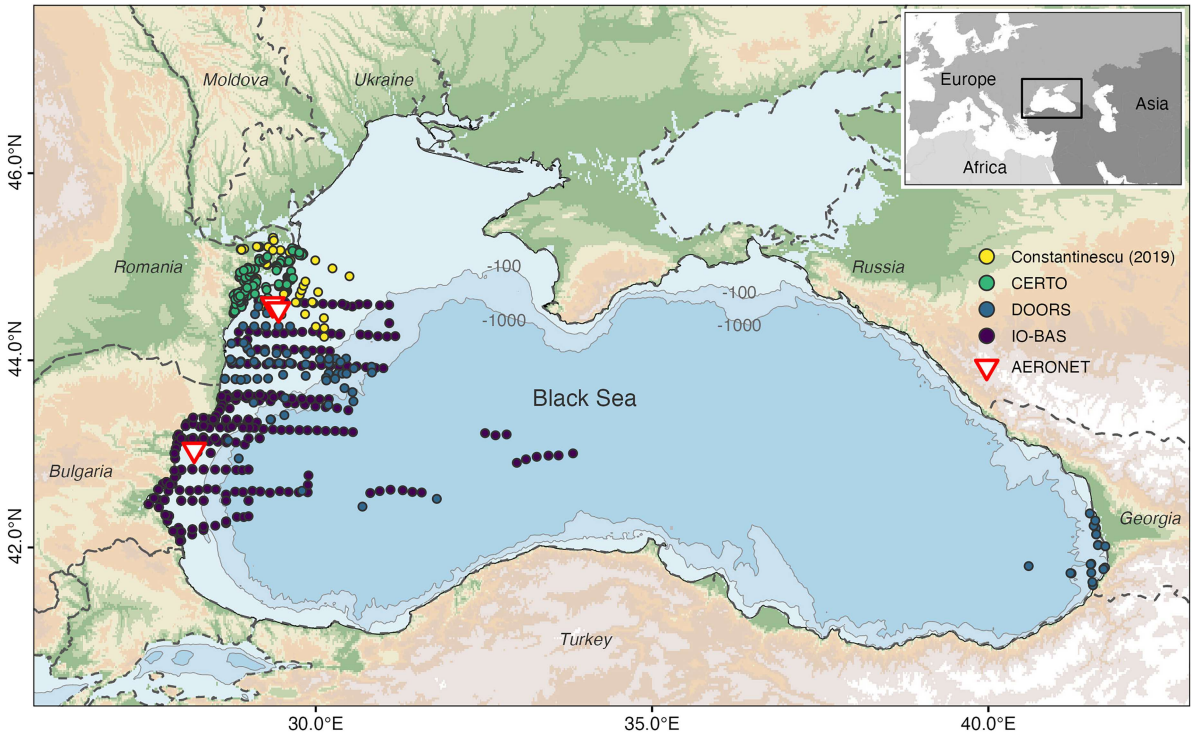

Figure 1. Locations of *in situ* data collected in this research. Point represents the location of *in situ* data, with color indicating the data source. Triangle indicates the location of the AERONET-OC platforms. Background bathymetry and elevation data were sourced from the General Bathymetric Chart of the Oceans (GEBCO), with gray solid lines and numbers indicating the water depth (m).

carried out following Jiang, Matsushita, and Yang (2020). Regarding AERONET-OC sites, automated above-water multi-spectral radiometry data (downwelling and upwelling radiances) are collected from fixed platforms, and processed data are made available online. In this study, we worked with Level-2 quality-controlled measurements of normalized water-leaving radiances (L_{wN}) corrected for bidirectional effects and referred to the nadir. These L_{wN} measurements were transformed to R_{rs} by dividing with the extra-solar irradiance spectrum (Zibordi et al. 2021). It should be noted that before 2018, the AERONET-OC spectral bands were adapted to MERIS, so 412 nm, 443 nm, 490 nm, 551 nm, 667 nm, and 870 nm were available for our validation exercise. After 2018, bands were adapted to OLCI with the addition of 400 nm, 510 nm, 620 nm, and 779 nm, and furthermore, the 551 nm and 870 nm bands were replaced by 560 nm and 865 nm, respectively.

All hyperspectral *in situ* R_{rs} data (i.e. HyperSAS and TriOS) were convolved into Sentinel-3 OLCI and Sentinel-2 MSI bands using their spectral response functions. For *in situ* R_{rs} measured using multi-spectral instruments (i.e. Profiler, AERONET-OC), R_{rs} were band shifted to the satellite bands using inverse and direct application of the Quasi-Analytical Algorithm (Mélin and Sclep 2015), similarly to several studies using the AERONET-OC data in the Black Sea (e.g. Zibordi et al. 2022; Zibordi, Mélin, and Berthon 2018).

2.2. Satellite matchup generation

The Copernicus Marine Service Ocean Color Thematic Assembly Center (CMEMS OCTAC) provides operationally daily consistently projected Level-3 ocean color variables (i.e. R_{rs}, Chl-a, $K_d(490)$) for the Black Sea at two spatial resolutions and temporal coverages: multi-sensor datasets (CMEMS MULTI) at 1 km, available from 1997 to present; and Sentinel-3 OLCI datasets (CMEMS OLCI) at 300 m from 2016 to present (Brando et al. 2024). The CMEMS MULTI R_{rs} timeseries is built from SeaWiFS, MODIS, MERIS, VIIRS-SNPP & JPSS1, Sentinel-3A and 3B OLCI sensors by merging the standard Level-2 R_{rs} data distributed by space agencies after applying inter-sensor bias correction and band shifting to the reference bands (Brando et al. 2024;

Colella et al. 2025). CMEMS OLCI merges directly, without bias correction or band shifting, Sentinel-3A and 3B OLCI Level-2 R_{rs} at full resolution (300 m) distributed by EUMETSAT (Brando et al. 2024). Chl-a retrieval for both datasets is based on a merging of two algorithms depending on the optical complexity of the water: a regional band ratio approach using two bands (490 nm and 555 nm) and a multilayer perceptron (MLP) neural network based on three bands (490 nm, 510 nm and 555 nm) (Kajiyama, D'Alimonte, and Zibordi 2018), with the band of 560 nm shifted to 555 nm for OLCI (Brando et al. 2024; Colella et al. 2025). A daily interpolated "gap-free" Level-4 Chl-a dataset (CMEMS INTERP) is also produced at 1 km resolution by using a modified version of the DINEOF algorithm (Brando et al. 2024; Volpe et al. 2018). $K_d(490)$ from CMEMS MULTI is computed using a 4th degree polynomial algorithm based on the R_{rs} band ratio between 490 nm and 510 nm, and applying the coefficients used in the NASA Ocean Biology Processing Group (OBPG) (Colella et al. 2025). In the case of the CMEMS OLCI, the standard Level-2 algorithm for $K_d(490)$ distributed by the EUMETSAT is directly implemented (Brando et al. 2024). Although all these datasets are available as NRT, we worked in this study with the multi-year (MY) datasets included in the CMEMS products OCEANCOLOUR_BLK_BGC_L3_MY_009_153 and OCEANCOLOUR_BLK_BGC_L4_MY_009_154 (Colella et al. 2025).

CERTO products are built from Sentinel-3 OLCI and Sentinel-2 MSI imagery freely provided through the Copernicus Data and Information Access Services (CREODIAS). To obtain R_{rs}, OLCI Level-1 data are atmospherically corrected by POLYMER v4.16 (Steinmetz, Deschamps, and Ramon 2011), while MSI Level-1 data are atmospherically corrected by combining outputs from POLYMER v4.16 and ACOLITE v20231023 (Vanhellemont and Ruddick 2018) to enhance accuracy across diverse water and atmospheric conditions, in particular for smaller area transitional water systems (Steinmetz and Ramon 2023; Van der Zande et al. 2024). The level-2 data from both sensors are masked using IdePix in SNAP 8 to remove land, cloud, and spurious data points with high uncertainty (Warren et al. 2019). OLCI and MSI R_{rs} were classified into 18 and 11 Optical Water Type (OWT) classes, respectively, based on the method from Atwood et al. (2024). For each sensor, the optimal performing water quality (Chl-a, TSM) estimation algorithm for each OWT class is selected (Jackson and Atwood 2022), and the algorithm outputs are blended using fuzzy-clustering membership to each OWT class as weights (Jackson, Sathyendranath, and Mélin 2017; Moore, Campbell, and Feng 2001). More details about Chl-a algorithm blending are described in Jackson and Atwood (2022) and that for TSM in Lin et al. (2026).

In addition, Chl-a and TSM concentrations available from the Sentinel-3 OLCI Level-2 Water Full Resolution (WFR) products processed by EUMETSAT within the baseline collection "OL_L2M.003" were also included in the validation exercise (EUMETSAT 2021). The EUMETSAT Chl-a concentration is derived from two methods: (1) OC4ME, a maximum band ratio semi-analytical chlorophyll algorithm developed by Morel et al. (2007) and a chlorophyll index (CI) approach applied in low-chlorophyll oligotrophic waters; and (2) Neural Network (NN), which is based on the Case 2 Regional Coast Color (C2RCC) NN v.2 for the retrieval of water inherent optical properties (IOPs) in optically complex waters. The EUMETSAT TSM concentration product was also produced by the C2RCC NN v.2 algorithm. Chl-a and TSM concentrations from Sentinel-3A and 3B were then resampled to the CMEMS OLCI geographical grid and merged to obtain a Level-3 dataset equivalent to the OLCI datasets distributed by the CMEMS. A summary of the ocean color products is provided in Table 2.

Satellite matchups, including R_{rs}, Chl-a, TSM, and $K_d(490)$ were generated for Sentinel-3 OLCI (2017–2024), Sentinel-2 MSI (2016–2024), and CMEMS MULTI (2011–2024) based on protocols proposed in the literature for medium- and high-spatial-resolution sensors (Concha, Bracaglia, and Brando 2021; EUMETSAT 2022). Specifically, the following methods and criteria were used for matchup generation:

(1) A 3 × 3-pixel window was used to extract data from satellite products for each *in situ* sampling location, and the median and standard deviation were calculated for the 9 pixels in this window;
(2) A matchup is considered valid when the number of valid values within the 3 × 3 window is not less than 5;
(3) The time difference between *in situ* sampling and satellite time must be less than 2 h, which was determined after checking different time windows against the ocean color product accuracy;
(4) All bands of *in situ*-measured R_{rs} must be positive, if there are any negative values in one *in situ* R_{rs} spectrum, then the whole spectrum was excluded from the validation dataset; while all satellite R_{rs}

Table 2. Summary of ocean color products validated in this research.

Source	Satellite sensor	Parameter	Spatial resolution	Algorithm	Reference
CMEMS	MULTI	R_{rs}	1 km	Sensor merging of standard L2 R_{rs}	Brando et al. (2024); Colella et al. (2025)
		Chl-a	1 km	Blended algorithm	Kajiyama, D'Alimonte, and Zibordi (2018)
		$K_d(490)$	1 km	Band ratio algorithm	Colella et al. (2025)
	INTERP	Chl-a	1 km	Interpolated	Brando et al. (2024) Volpe et al. (2018)
	OLCI	R_{rs}	300 m	Standard Level 2	EUMETSAT (2021)
		Chl-a	300 m	Blended algorithm	Kajiyama, D'Alimonte, and Zibordi (2018)
		$K_d(490)$	300 m	Band ratio algorithm	Colella et al. (2025)
EUMETSAT	OLCI	Chl-a	300 m	OC4ME	EUMETSAT (2021)
			300 m	Neural network	EUMETSAT (2021)
		TSM	300 m	Neural network	EUMETSAT (2021)
CERTO	OLCI	R_{rs}	300 m	POLYMER	Steinmetz and Ramon (2023); Steinmetz, Deschamps, and Ramon (2011)
		Chl-a	300 m	Blending based on OWT	Atwood et al. (2024); Jackson and Atwood (2022)
		TSM	300 m	Blending based on OWT	Atwood et al. (2024); Lin et al. (2026)
	MSI	R_{rs}	60 m	POLYMER and ACOLITE	Steinmetz and Ramon (2023); Steinmetz, Deschamps, and Ramon (2011), Vanhellemont and Ruddick (2018)
		Chl-a	60 m	Blending based on OWT	Atwood et al. (2024); Jackson and Atwood (2022)
		TSM	60 m	Blending based on OWT	Atwood et al. (2024); Lin et al. (2026)

including negatives were retained so that a comprehensive evaluation of the R_{rs} products can be achieved;

(5) *In situ* Chl-a must be larger than 0.01 mg/m^3, to avoid any values below the instrument detectability threshold, which can lead to potential errors in the validation.

Satellite time was fixed to 11:00 UTC for the CMEMS-MULTI products. In case of the CMEMS OLCI, CERTO OLCI and CERTO MSI, the satellite time was taken from the metadata from the satellite images. In addition, we only selected AERONET-OC R_{rs} data, which have the same number of valid data across the spectra, to ensure that the number of valid R_{rs} are same for each AERONET-OC band and the validation results comparable between the AERONET-OC bands.

2.3. Accuracy assessment

The root mean square deviation (RMSD), mean absolute percentage deviation (MAPD), and Bias were used to quantify product accuracy. The slope and R^2 of linear regression analysis were also included.

$$\mathrm{RMSD} = \sqrt{\frac{\sum_{i=1}^{N}(X_{\mathrm{estimated},i} - X_{\mathrm{measured},i})^2}{N}}, \tag{1}$$

$$\mathrm{MAPD} = \mathrm{mean}\left(\left|\frac{X_{\mathrm{estimated},i} - X_{\mathrm{measured},i}}{X_{\mathrm{measured},i}}\right| \cdot 100\%\right), \tag{2}$$

$$\mathrm{Bias} = \frac{\sum_{i=1}^{N}(X_{\mathrm{estimated},i} - X_{\mathrm{measured},i})}{N}. \tag{3}$$

where X_{measured} is the *in situ* data, $X_{\mathrm{estimated}}$ is the corresponding satellite-derived value, and N is the number of data points.

3. Results

3.1. Bio-optical characteristics

A total number of 363 *in situ* R_{rs} spectra were collected from field campaigns in the Black Sea. There are more than two thousand spectra available from the three AERONET-OC sites since 2011, but the number of spectra finally used for validation varied between products: CMEMS MULTI ($N = 1370$), CMEMS OLCI

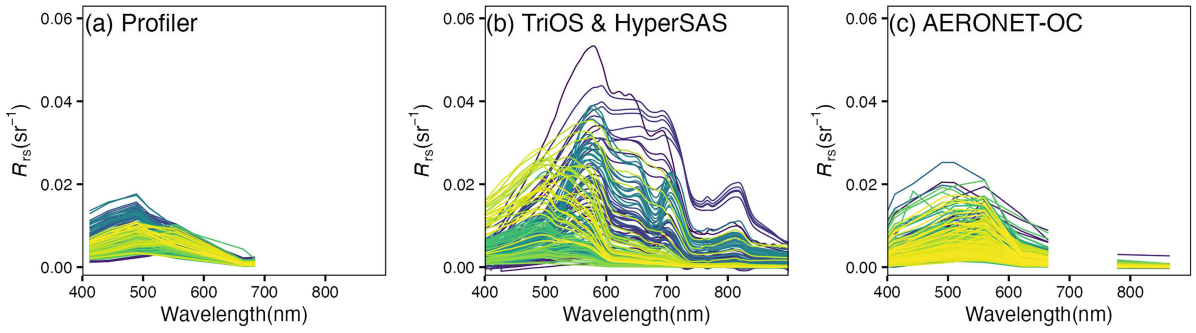

Figure 2. Remote sensing reflectance (R_{rs}) spectra collected from (a) Profiler, (b) TriOS and HyperSAS, and (c) AERONET-OC sites in the Black Sea. The color indicates the spectra from different stations or dates.

($N = 706$), CERTO OLCI ($N = 831$), and CERTO MSI ($N = 175$) after quality control and matching with satellite data, as detailed in Section 2.2. Our collected spectra presented a wide range of shapes and magnitudes covering clear and turbid waters (Figure 2), with the magnitude of R_{rs} at 560 nm ranging from 0.001 sr^{-1} to 0.05 sr^{-1}. High spectra with $R_{rs}(560) > 0.02$ sr^{-1} were collected from the Danube Delta and Georgian coast. As shown in Figure 2, these spectra showed either R_{rs} peaks at around 700 nm, indicating high phytoplankton biomass, or peaks at around 810 nm, indicating high sediments in the water.

There are 759 *in situ* Chl-a concentration data ranging from 0.02 mg/m^3 to 121.9 mg/m^3, with an average value of 8.4 mg/m^3, and median value of 1.1 mg/m^3 (Figure 3b). A clear spatial pattern was observed for Chl-a (Figure 3a), which shows a decrease trend from the western coast to the central Black Sea, and

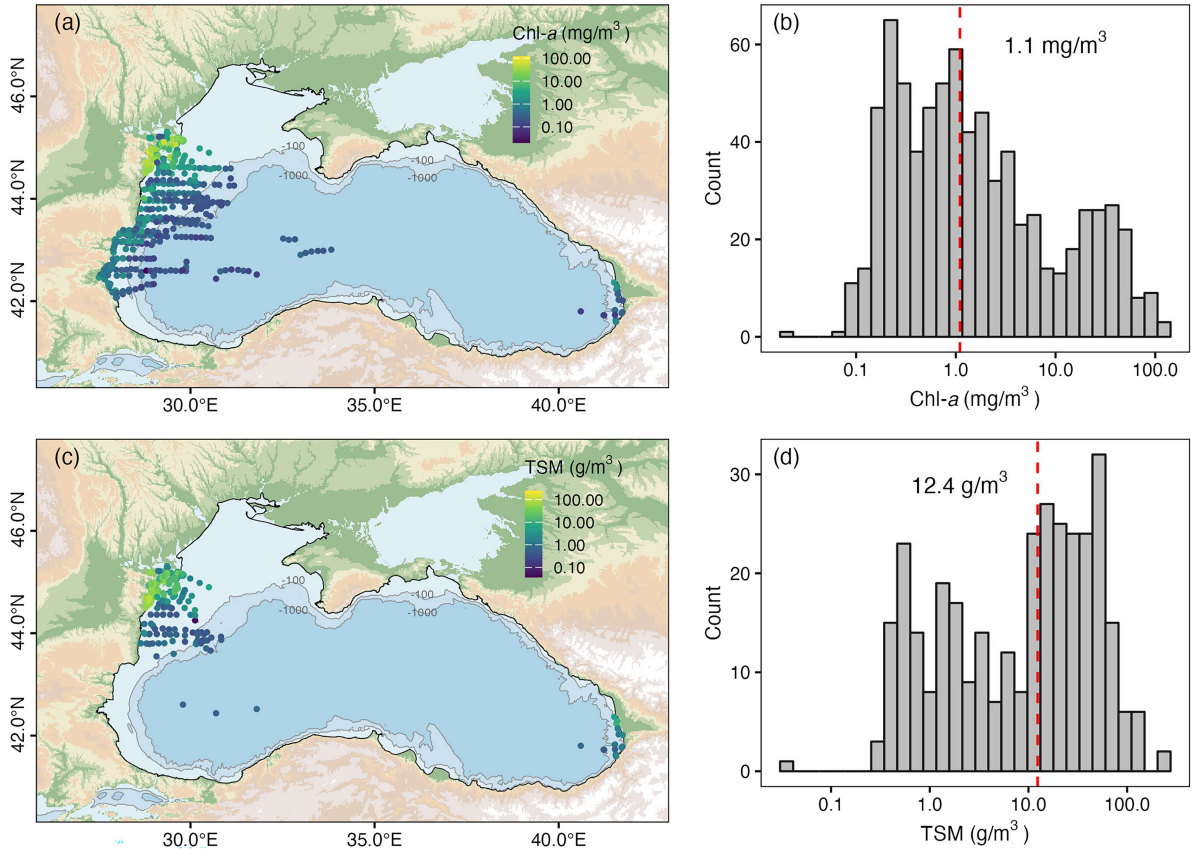

Figure 3. Chl-a and TSM distributions in the *in situ* dataset. (a) Map of *in situ* Chl-a, (b) histogram of *in situ* Chl-a, (c) map of *in situ* TSM, and (d) histogram of *in situ* TSM. The red dashed line in the histogram plots represents the median value of Chl-a and TSM.

becomes lower from the north (Danube Delta) to the south of the Black Sea. All samples with Chl-a higher than 10 mg/m^3 were collected from Danube Delta regions, including lakes, lagoons, and coastal waters. *In situ* TSM data ranged from 0.04 g/m^3 to 245 g/m^3, with an average value of 22.9 g/m^3 and a median of 12.4 g/m^3 (Figure 3d). The TSM showed a similar spatial pattern as Chl-a (Figure 3c), and high TSM appeared mainly in lakes, lagoons, and coastal waters of the Danube Delta region in the western Black Sea, and coastal waters near Georgia in the eastern Black Sea. In addition, we compiled 218 $K_d(490)$ data (Table 1) ranging from 0.02 m^{-1} to 0.84 m^{-1}, with an average of 0.17 m^{-1} and a median of 0.11 m^{-1}, and a similar spatial pattern as TSM was observed.

3.2. R_{rs} product

Validation of the CMEMS MULTI R_{rs} was based on *in situ* data from all the sources collected between 2011 and 2024, resulting in 1438 valid matchups, including 36 spectra from Profiler, 32 from TriOS and HyPerSAS, and 1370 from the AERONET-OC sites. The band of 670 nm has significant smaller number of matchups ($N = 163$) because data were not available from Section-7, only available until 2018 for Gloria, and only available between 2014 and 2021 for Galata.

CMEMS MULTI presented overall accurate R_{rs} values across blue–green–red bands, with all MAPD lower than 30%, except for the short-blue band of 412 nm (Figure 4). The bands between 490 and 555 nm showed higher accuracies than the other bands, with the lowest MAPD of 11.11% at 555 nm, indicating the reliability of R_{rs} at these bands from the MULTI products. However, some underestimations were observed in turbid waters. For instance, when $R_{rs}(555)$ was higher than 0.015 sr^{-1}, and $R_{rs}(670)$ was higher than 0.01 sr^{-1}.

Matchups for the CMEMS OLCI R_{rs} validation included 16 spectra measured by Profiler, 26 by TriOS and HyperSAS, and 706 by AERONET-OC platforms. For simplification and better comparison with other satellite sensors, we used integers of the OLCI central wavelengths (e.g. 413 nm rather than 412.5 nm). Because band availabilities varied between these instruments, this resulted in a maximum number of matchups for bands 413, 443, 490, 510, 560, and 665 nm ($N = 748$), with data available from all three instruments, and was

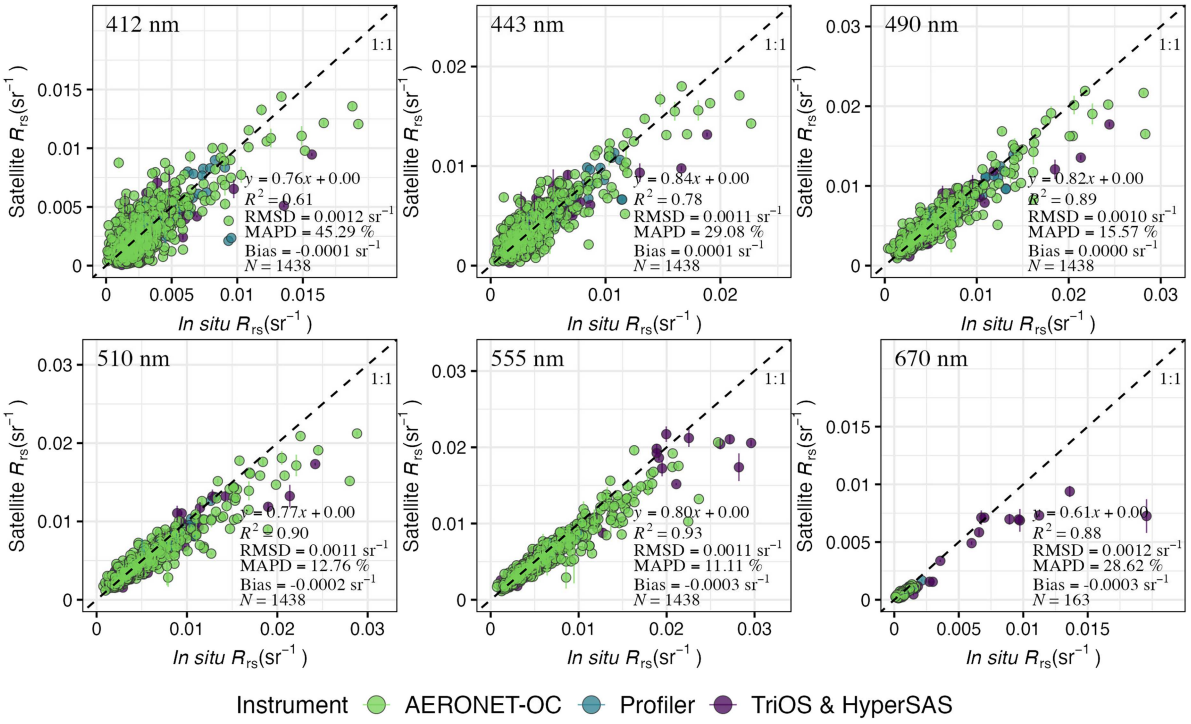

Figure 4. Validation of R_{rs} for CMEMS MULTI products. Vertical bar represents one standard deviation of each data point within the 3 × 3-pixel window. The color represents the instrument (or platform) used for measuring R_{rs}.

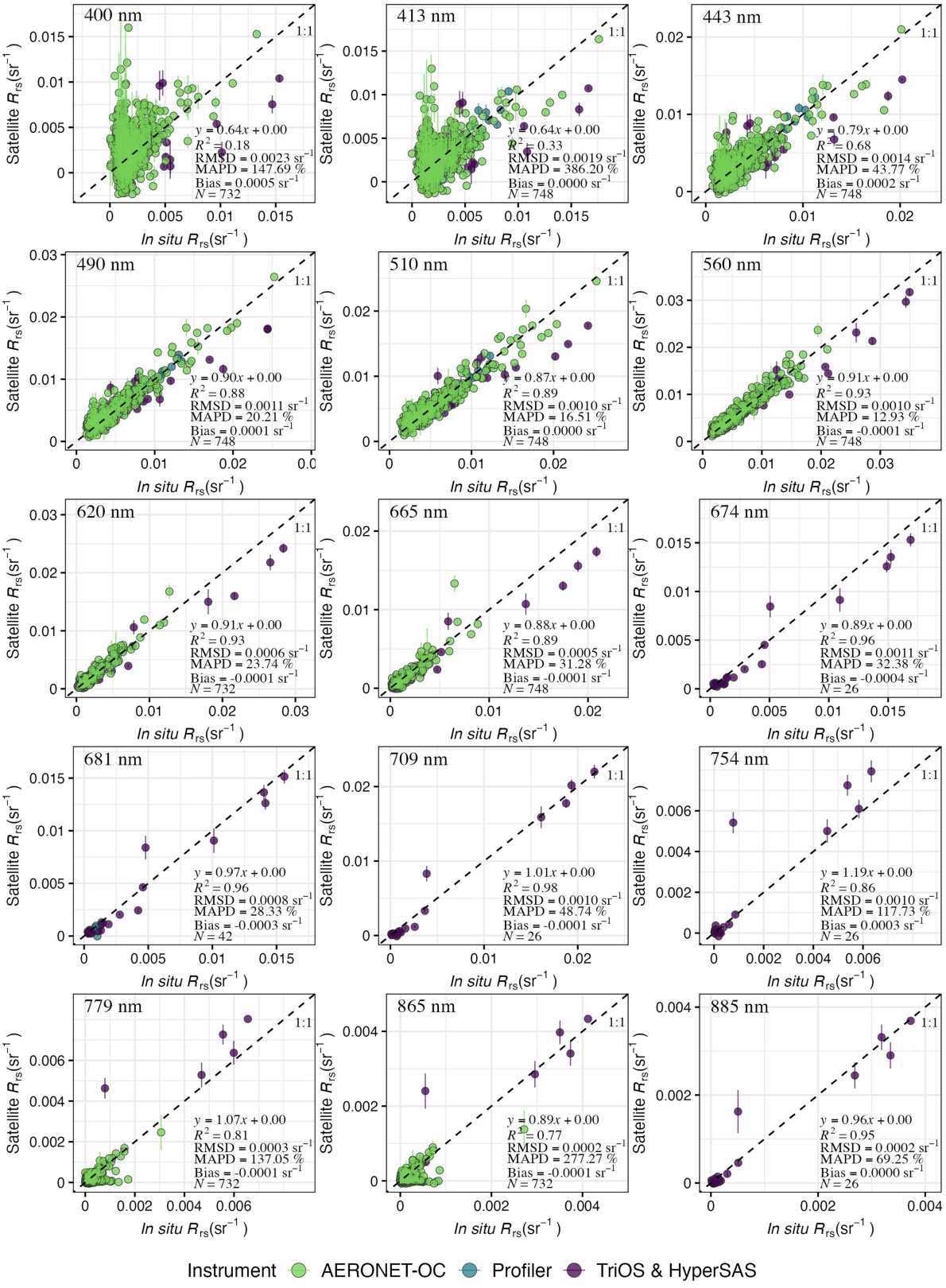

Figure 5. Validation of R_{rs} for CMEMS OLCI products. The vertical bars represent one standard deviation within the 3 × 3-pixel window. The color represents the instrument (or platform) used for measuring R_{rs}. Bands at 754 nm and 885 nm are produced internally but not distributed by CMEMS.

the lowest for bands 674, 709, 754, and 885 nm ($N = 26$), as these bands were only available from TriOS and HyperSAS (Figure 5).

The accuracy of OLCI R_{rs} from the CMEMS varied at different bands, with generally more accurate results in visible bands (between 490 and 681 nm) with a MAPD lower than 35% and R^2 higher than 0.88 (Figure 5). The highest accuracy was found for 560 nm with a MAPD of 12.93%. R_{rs} at shortwave blue bands (400 and 413 nm) showed larger errors than other bands, with MAPD higher than 100%. R_{rs} at near-infrared (NIR) bands from 754 nm to 885 nm presented slightly larger errors compared to visible bands, with some underestimations observed, particularly in clear waters, where R_{rs} comes close to zero (e.g. 779 nm and 865 nm).

The number of valid R_{rs} matchups obtained from CERTO OLCI is higher than the one from the CMEMS OLCI for all spectral bands, with a maximum of 883 matchups for bands at 413, 443, 490, 510, 560, and 665 nm (Figure 6). This consisted of 15 *in situ* spectra from Profiler, 37 from TriOS and HyperSAS, and 831 from AERONET-OC. Similar to the CMEMS OLCI, the number of matchups varies between bands due to the band availability of the different instruments.

OLCI R_{rs} from CERTO presented high accuracy in visible bands between 443 nm and 665 nm, with all MAPD lower than 30% and R^2 higher than 0.88 across clear and turbid waters (Figure 6). The most accurate band is 560 nm, with a MAPD of 10.43%. Similar to CMEMS OLCI R_{rs} products, CERTO OLCI R_{rs} at 400 nm and 413 nm showed larger errors, with MAPD higher than 50%, as well as underestimations for low values and overestimations for high values being observed. For the NIR bands from 709 nm to 885 nm, larger errors were found compared to visible bands, with slight underestimations in turbid waters, and many negative R_{rs} particularly at 709 nm, 865 nm and 885 nm.

Although CERTO MSI shows a lower coverage as compared to the CMEMS MULTI and OLCI datasets, we were able to obtain up to 190 matchups for all the bands from 443 nm to 665 nm, which consist of 4 *in situ* spectra from Profiler, 11 from TriOS and HyperSAS, and 175 from AERONET-OC. Bands 705 and 740 nm have only 11 matchups, as they are only available from TriOS and HyperSAS.

MSI R_{rs} from CERTO showed the highest accuracy at 560 nm, with a MAPD of 13.97% (Figure 7). R_{rs} at 443 nm, 490 nm and 665 nm showed slightly overestimations, but all R^2 were higher than or equal to 0.75, and the regression slopes were higher than 0.80. R_{rs} at NIR bands (>700 nm) generally exhibited underestimations for turbid waters, and some negative values were observed in clear waters with low R_{rs} values.

3.3. Water quality products

There are seven Chl-a products from CMEMS, EUMETSAT, and CERTO, but each with different number of matchups, ranging from 28 for CERTO MSI to 263 for CMEMS INTERP (Figure 8). The variations were due mainly to differences in masking during data processing and the spatial resolution of the satellite images. CMEMS INTERP provided a significantly greater number of matchups than other products due to the temporal and spatial interpolation, including twelve Level-3 daily images, and gap filling using climatology values (Colella et al. 2025). Considering only the products from OLCI, CERTO provided a remarkably higher number of valid matchups (109) as compared to CMEMS or EUMETSAT OC4ME (73) or EUMETSAT NN (90). CERTO MSI shows the lowest number of matchups because of the longer revisit time of the Sentinel-2 satellite.

Chl-a from CMEMS OLCI showed the highest accuracy, with a MAPD of 56.22% and bias of 0.13 mg/m^3(Figure 8b). The CMEMS MULTI and INTERP Chl-a products presented good agreements with *in situ* values in clear waters, but more scattered in turbid waters when *in situ* Chl-a is higher than 10 mg/m^3 (Figures 8a and 8c). The two Chl-a products from EUMETSAT showed larger errors (MAPD > 150%) than the others (Figures 8d and 8e), with the neural network overestimating when *in situ* Chl-a lower was than 1 mg/m^3 and underestimating when higher than 10 mg/m^3. The OC4ME Chl-a was consistently overestimated across the validation range. Chl-a products from CERTO showed good agreement with *in situ* data in turbid waters but slight overestimations in clear waters when *in situ* Chl-a was lower than 1 mg/m^3(Figures 8f and 8g).

Three TSM products were validated in this research: EUMETSAT OLCI, CERTO OLCI and CERTO MSI. CERTO OLCI (Figure 9b) has 21 more TSM matchups than EUMETSAT OLCI (Figure 9a), and they presented good comparable accuracy, with a lower RMSD (13.80 g/m^3 vs 28.98 g/m^3) and bias (−1.90 g/m^3 vs −6.58 g/m^3)

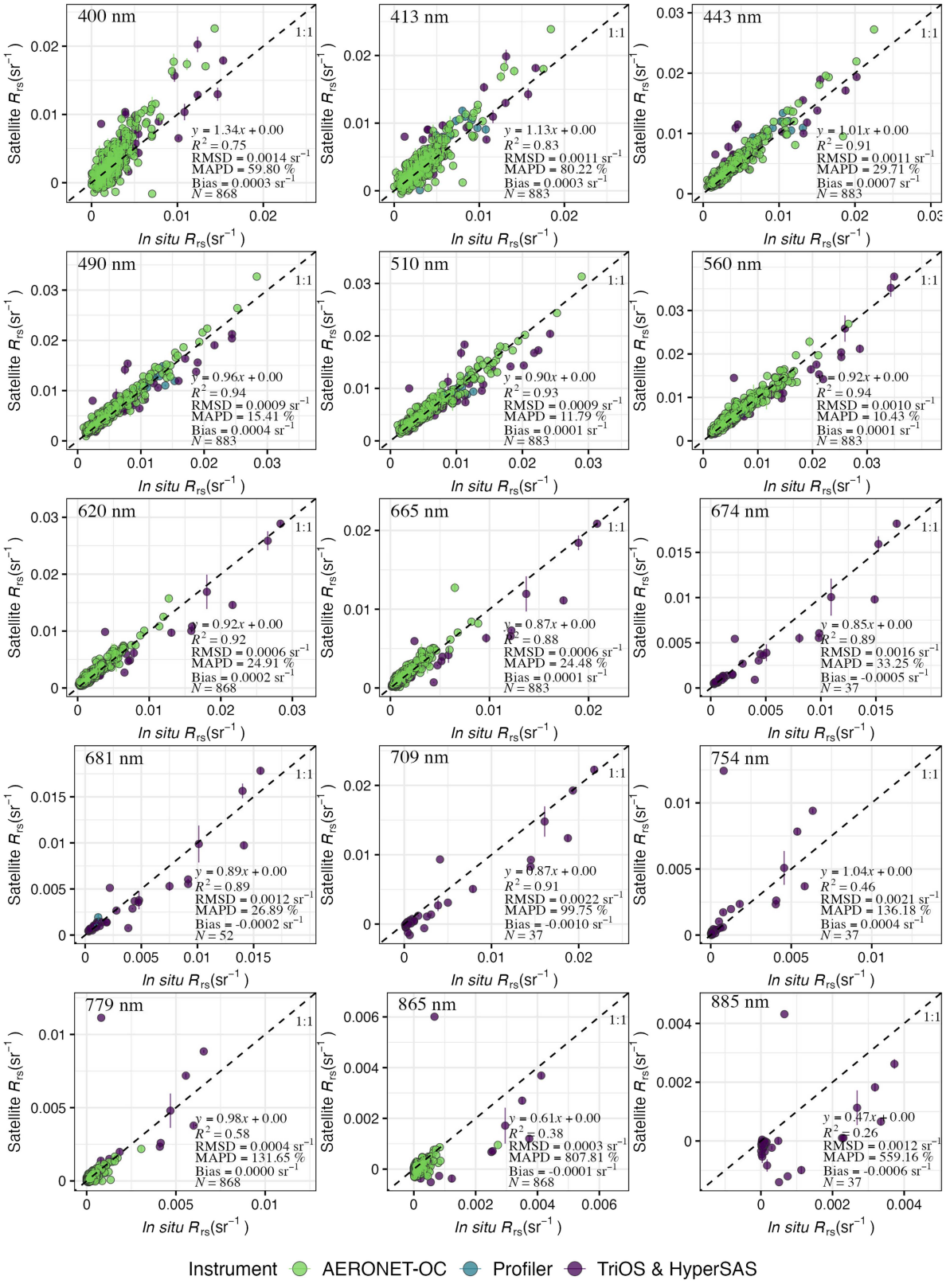

Figure 6. Validation of R_{rs} for CERTO OLCI products. The vertical bars represent one standard deviation within the 3 × 3-pixel window. The color represents the instrument (or platform) used for measuring R_{rs}.

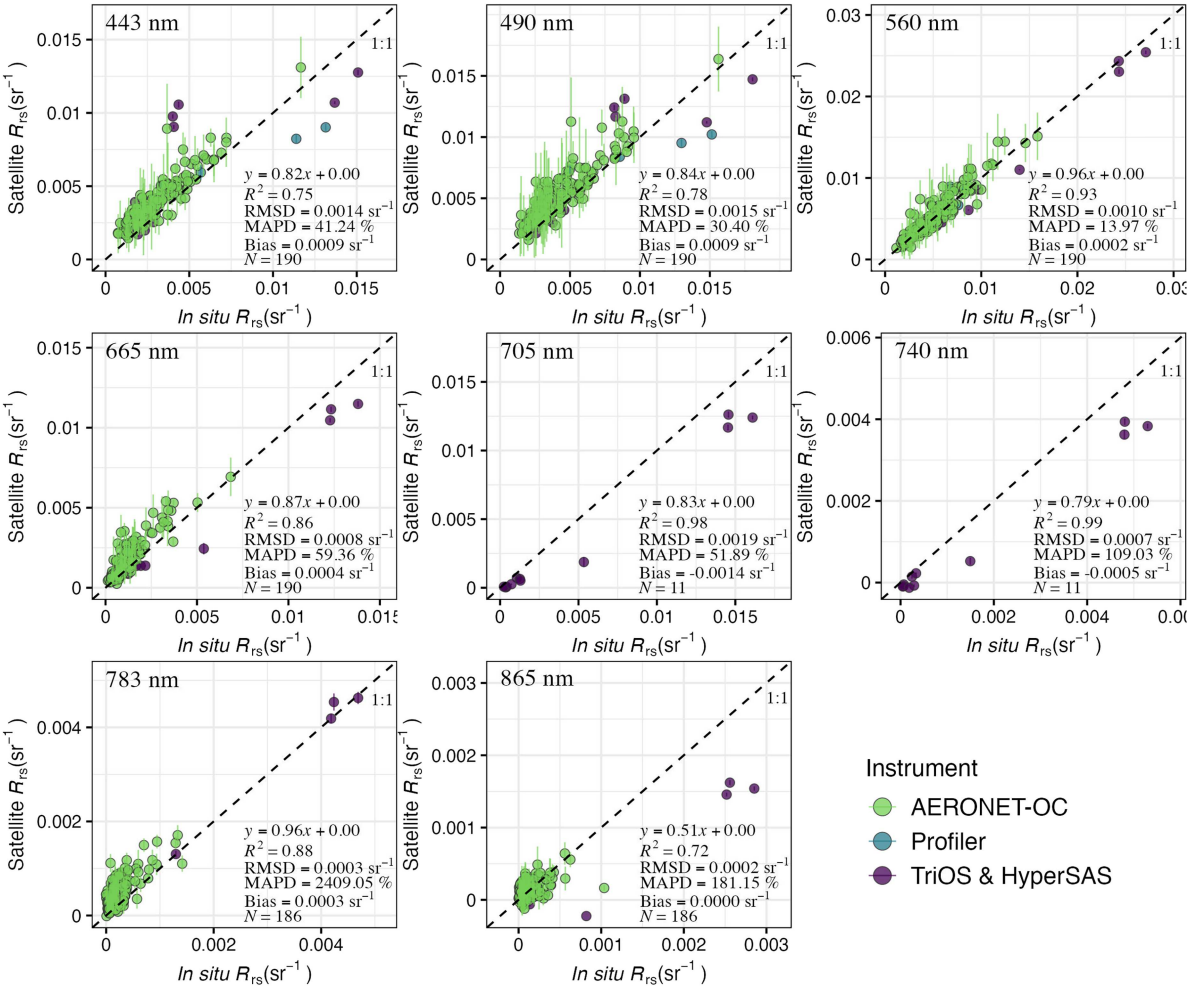

Figure 7. Validation of R_{rs} for CERTO MSI products. The vertical bars represent one standard deviation within the 3 × 3-pixel window. Color represents the instrument (or platform) used for measuring R_{rs}.

from EUMETSAT but a lower MAPD from CERTO (70.47% vs 47.29%). CERTO MSI has only 18 TSM matchups because of the smaller spatial and temporal coverages (Figure 9c), showing the smallest MAPD (45.65%) among all TSM products, although a few underestimated values in turbid waters were observed.

There are 21 more K_d(490) matchups from CMEMS MULTI than from OLCI. Both products presented an accuracy with a MAPD lower than 20% and RMSD lower than 0.1 m^{-1} and agreed with *in situ* measurements in both clear and turbid waters (Figure 10).

3.4. Comparison between CMEMS, CERTO, and EUMETSAT OLCI products

Only OLCI ocean color products are available across the CMEMS, EUMETSAT and CERTO. In terms of coverage, a larger number of valid matchups is obtained from CERTO for R_{rs}, Chl-a, and TSM datasets (see Figures 5, 6, 8, and 9). These discrepancies are explained by the different atmospheric correction processors and flagging schemes.

To compare the accuracy of ocean color products between the CMEMS, EUMETSAT, and CERTO, we compiled the common matchups of R_{rs}, Chl-a, and TSM (i.e. matchups available from all products on the same date and site to exclude the influence of using different data flagging). We found that R_{rs} from CERTO presented slightly higher accuracy than CMEMS at bands 400–665 nm, 754 nm and 779 nm, while CMEMS provided more accurate R_{rs} at the other mostly NIR bands (Figure 11).

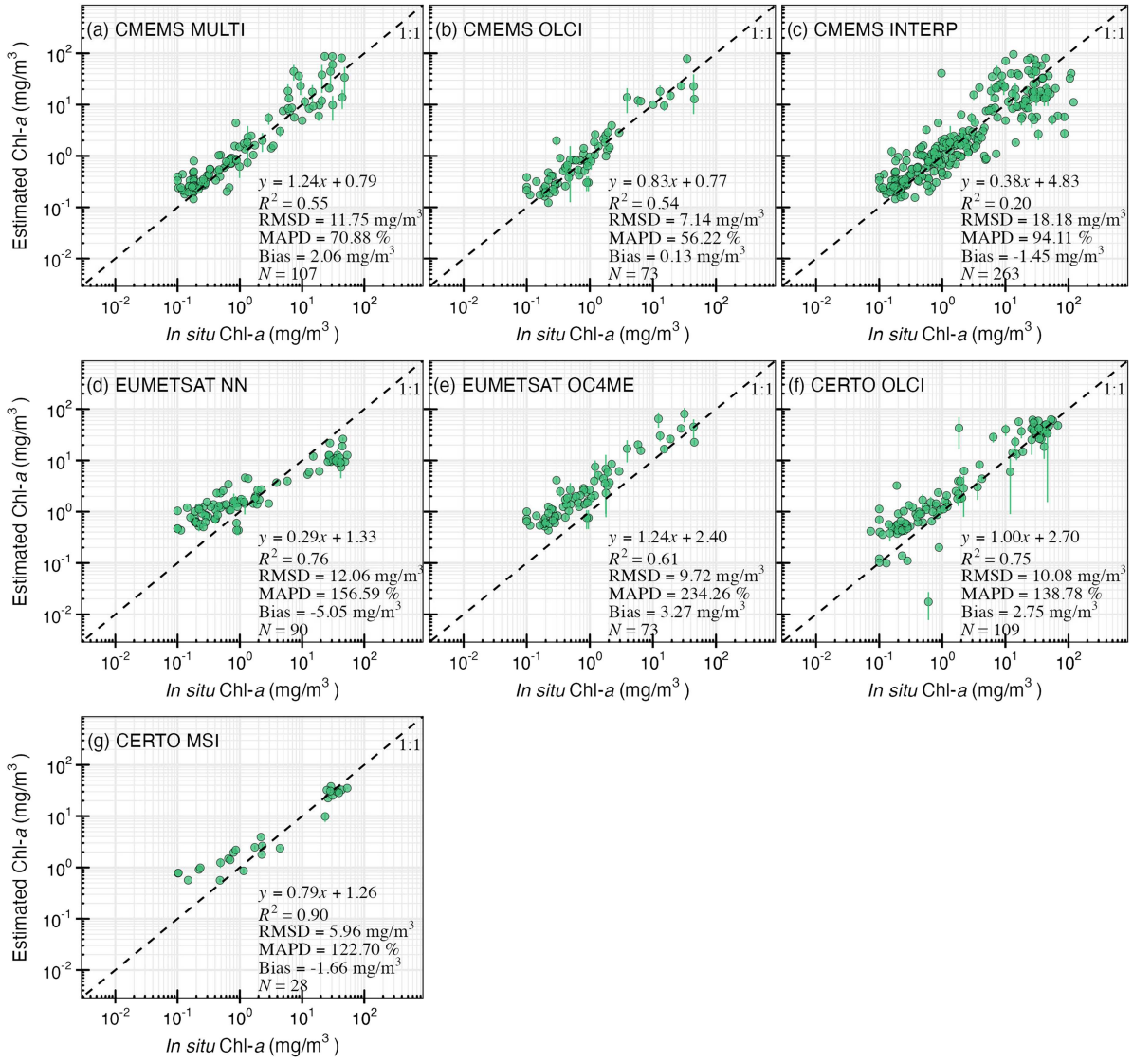

Figure 8. Validation of Chl-*a* products from (a) CMEMS MULTI (N=107), (b) CMEMS OLCI (N=73), (c) CMEMS INTERP (N=263), (d) EUMETSAT NN (N=90), (e) EUMETSAT OC4ME (N=73), (f) CERTO OLCI (N=109), and (g) CERTO MSI (N=28).

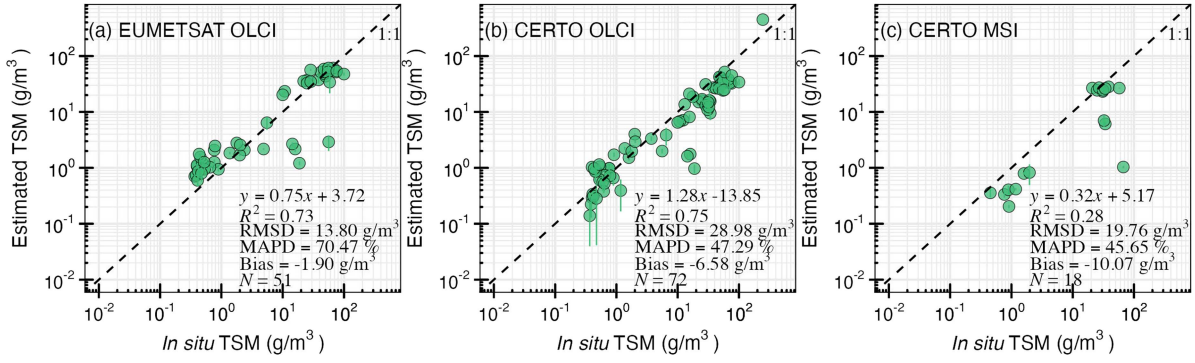

Figure 9. Validation of TSM products from (a) EUMETSAT OLCI (N=51), (b) CERTO OLCI (N=72), and (c) CERTO MSI (N=18).

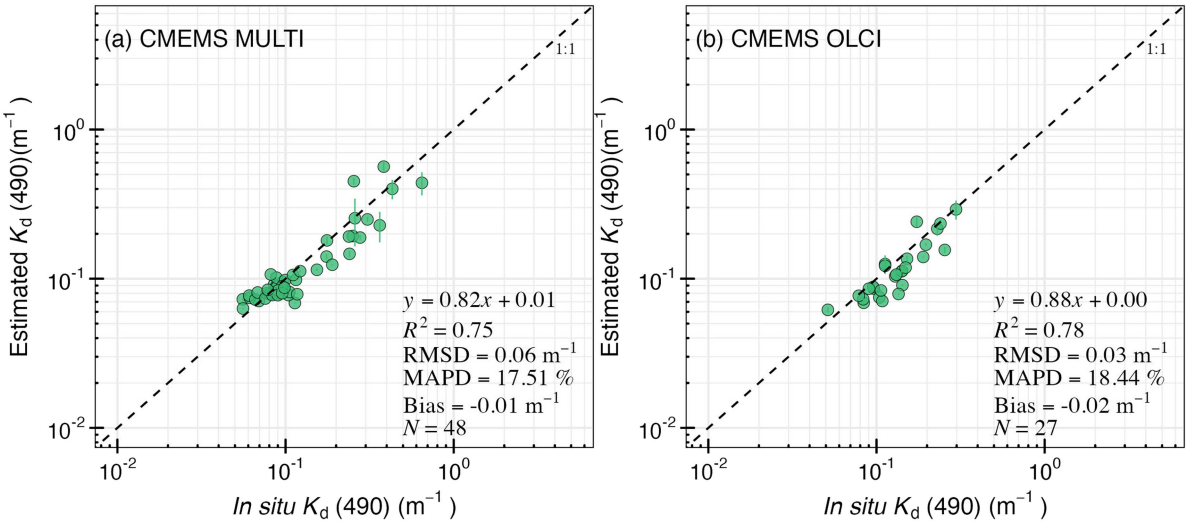

Figure 10. Validation of K_d(490) products from (a) CMEMS MULTI (N=48) and (b) CMEMS OLCI (N=27).

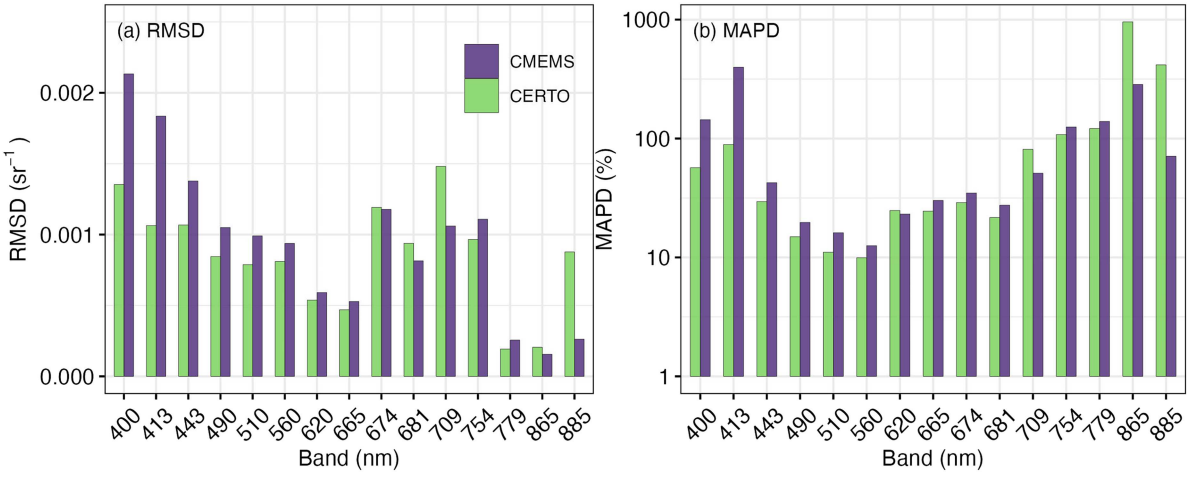

Figure 11. Comparison of RMSD and MAPD between CMEMS and CERTO OLCI R_{rs} products.

We obtained 60 common Chl-a matchups between the CMEMS and CERTO OLCI products covering clear and turbid waters, as indicated by the CERTO OWT classes from 1 (clear) to 18 (turbid) in Figure 12. Both of the satellite-derived Chl-a agreed with the *in situ* measurements, with points aligning along the 1:1 line and further indicated with slope higher than 0.80. Slight overestimations were observed for CERTO OLCI Chl-a when *in situ* Chl-a was lower than ~10 mg/m^3 (Figure 12b). Comparing the performance between different OWT classes, CERTO OLCI Chl-a has higher accuracy in OWTs 4, 8, 12, and 18, and CMEMS OLCI Chl-a higher in the other OWTs (Figure 13).

In case of TSM, we compared the CERTO product with the EUMETSAT dataset (Figure 14). We obtained the opposite results as compared to Chl-a, with EUMETSAT provided more accurate estimates in turbid waters and CERTO with higher accuracy in clear waters. Overall, both provided accurate results, except for a few scattered points in medium turbid waters with *in situ* TSM at around 20 g/m^3. When comparing accuracy between different CERTO OLCI showed better estimates for OWTs 1, 2, 3, 6, 7, 9, 10, 12, 13, 14, 15, and 16, which are mainly in clear waters. EUMETSAT OLCI performed better in waters for OWTs 4, 5, 17, and 18 (Figure 15).

3.5. Showcase of ocean color products

An example of CMEMS OLCI, CMEMS MULTI, CMEMS INTERP, and CERTO OLCI Chl-a products on 23 May 2019 covering the Danube Delta region in the Black Sea is shown in Figure 16. All four products consistently

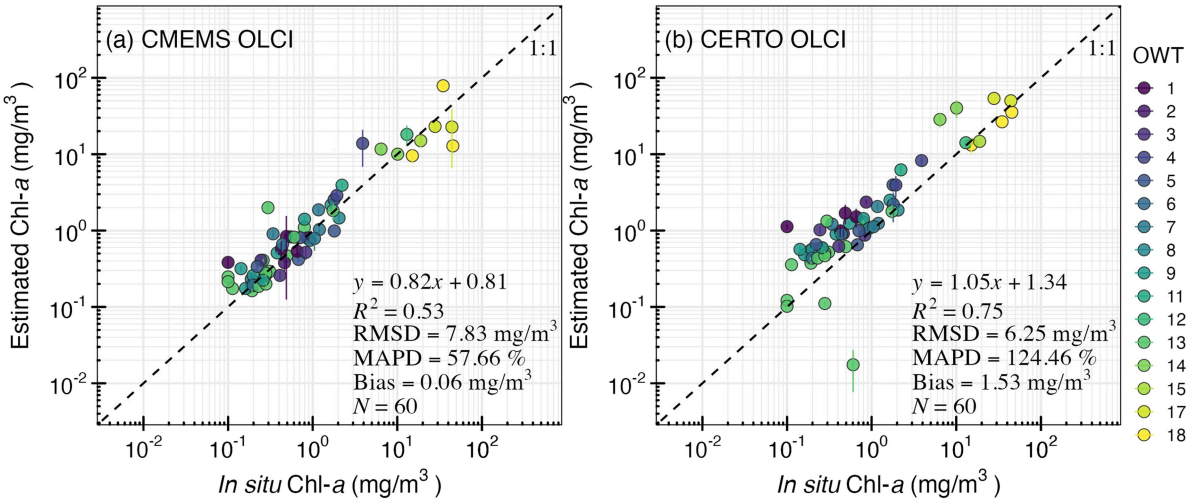

Figure 12. Validation of Chl-a between CMEMS and CERTO OLCI products. The color represents the OWT identified in CERTO products.

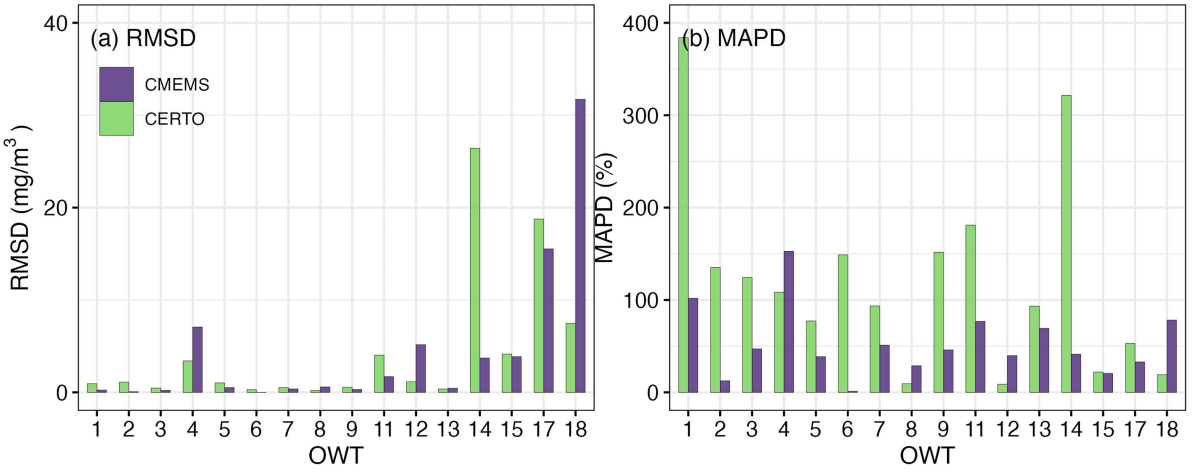

Figure 13. Comparison of RMSD and MAPD between CMEMS and CERTO OLCI Chl-a products in different optical water types (OWTs).

showed high Chl-a near the coast and low Chl-a offshore. However, some differences were observed. First, the range of Chl-a from the CMEMS OLCI (0.07 to 99.98 mg/m^3) was larger than that of the other three products (e.g. CMEMS MULTI between 0.13 and 44.28 mg/m^3), with higher Chl-a values in coastal turbid waters (Region A in Figure 16) and lower values in offshore clear waters (Region B in Figure 16, Table 3). This agreed with the results in Figures 8 and 12, with the CMEMS MULTI, CMEMS INTERP, and CERTO OLCI showing slightly higher Chl-a estimates than the CMEMS OLCI in clear waters. Second, the spatial coverage between the four Chl-a products are different, as Region C indicated in Figure 16. The CMEMS MULTI (covered 84.10% of Region C area) showed wider coverage than CMEMS OLCI (52.37%) and CERTO OLCI (53.16%), as would be expected to benefit from merging multiple satellite image sources. CMEMS INTERP further improved the spatial coverage by filling the data gaps (99.89%, Table 3).

Remarkable differences between OLCI products are also observed in Region D: some white pixels are seen in CMEMS (Figure 16a) because Chl-a was not produced, whereas a more spatially consistent Chl-a map was created for CERTO (Figure 16d). Discrepancies are explained by the different atmospheric correction processors: POLYMER (CERTO) managed to provide reliable R_{rs} data throughout the whole

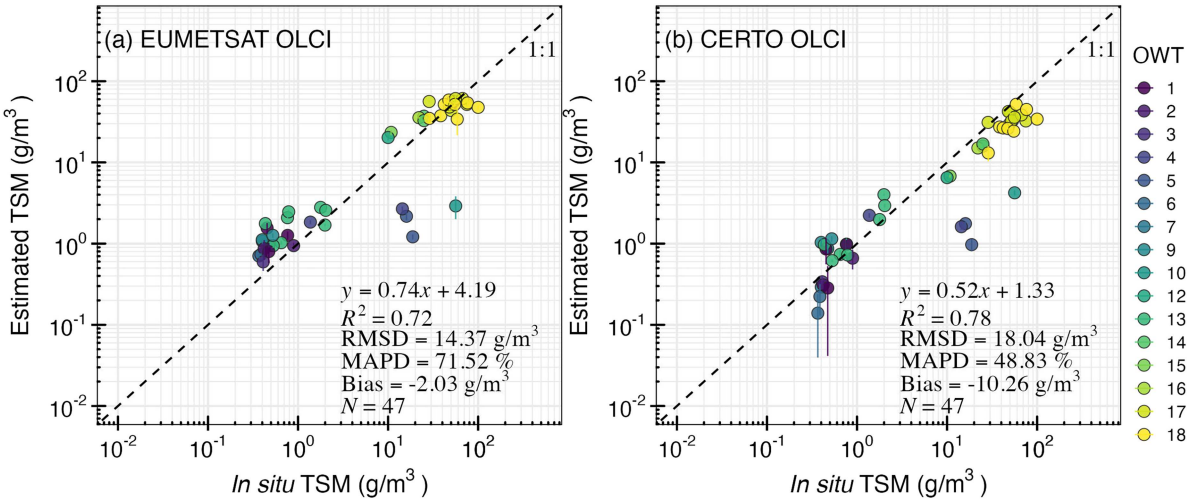

Figure 14. Validation of TSM between EUMETSAT and CERTO OLCI products. The color represents the OWT identified in CERTO products.

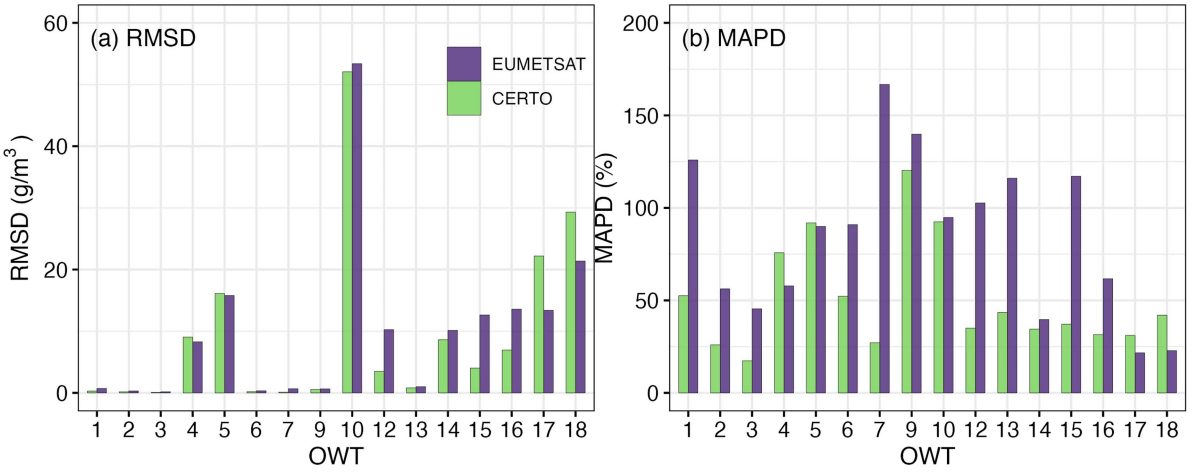

Figure 15. Comparison of RMSD and MAPD between EUMETSAT and CERTO OLCI TSM products in different optical water types (OWTs).

area, but WFR (CMEMS) produced some pixels with negative R_{rs} values that were flagged prior to Chl-a computation. The CMEMS MULTI product (Figure 16b) also shows good values, as the NASA Level-2 R_{rs} products deliver non-negative values.

To illustrate differences in the success rates of valid data between different products, a comparison on the number of negative and valid R_{rs} spectra between the CMEMS and CERTO are provided in Table 4. A negative spectrum was defined as a satellite spectrum that has one or more negative bands. The comparison was carried out for the period of 01 July 2016–30 June 2024 (2922 days), when all products were available, and all AERONET-OC bands were included. An initial comparison for all available bands from each product revealed that the CMEMS MULTI provides the highest success rate of 69.92%, with no negative R_{rs}. CERTO OLCI and MSI have a success rates lower than 10%, as there were many negative R_{rs}, especially in the NIR bands (Figures 6 and 7). However, when comparing only the six bands that all the CMEMS and CERTO products have available and are widely used for Chl-a retrieval (e.g. OC4ME), CERTO OLCI provided 12.5% more valid R_{rs} than CMEMS OLCI as CMEMS has more negative spectra than CERTO (93 vs 14). This explains why CERTO OLCI provides better spatial coverage than CMEMS OLCI in Figure 16.

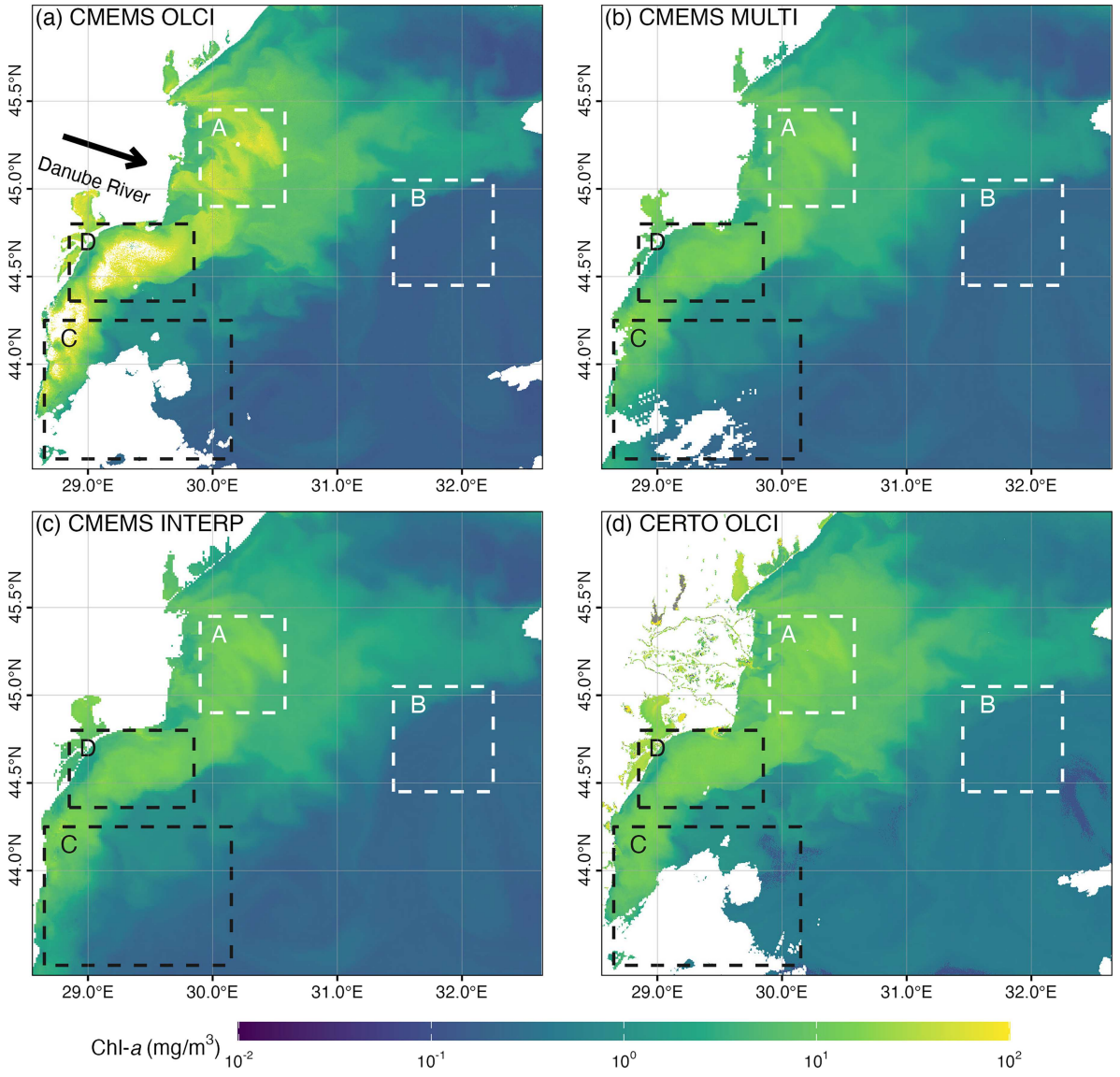

Figure 16. Examples of Chl-a product on 23 May 2019 in the Danube Delta region of the western Black Sea from (a) CMEMS OLCI, (b) CMEMS MULTI, (c) CMEMS INTERP, and (d) CERTO OLCI. Regions A and B indicate high and low Chl-a areas, respectively. Region C indicates the influence of Chl-a retrieval by clouds, and Region D differences in atmospheric correction processors.

4. Discussion

4.1. Advantages and limitations of the validation work

In this research, we compiled a comprehensive *in situ* dataset from the Black Sea to validate the ocean color products provided by the CMEMS, CERTO, and EUMETSAT. The *in situ* dataset covered wide spatial and bio-optical ranges, including turbid waters in the Danube Delta with high sediment loading from the Danube River, shallow (average depth of around 2 m and shallowest less than 1 m) productive waters in the Razelm–Sinoe Lagoon to the South of the Danube Delta, and deep (>1000 m) clear waters from the central Black Sea. Particularly, we collected novel optical and biogeochemical data from the Georgian coast, a region from which such a complete dataset has not yet been reported. Other studies have focused on particular characteristics of the Black Sea water environment, such as microbial water quality in Georgian coastal waters using *in situ* data (Janelidze et al. 2011), phytoplankton monitoring using Earth observations in the Black Sea (Kopelevich et al. 2014; Vostokov, Vostokova, and Vazyulya 2022; Yunev et al. 2021), and

Table 3. Summary of Chl-a values and the spatial coverage of valid data in the four regions indicated in Figure 16.

Region	Product	Median Chl-a (mg/m^3)	CV (%)	Spatial coverage (%)
A	CMEMS OLCI	21.71	62.31	99.77
	CMEMS MULTI	9.65	37.08	100.00
	CMEMS INTERP	9.65	37.08	100.00
	CERTO OLCI	12.00	29.09	99.99
B	CMEMS OLCI	0.18	99.37	100.00
	CMEMS MULTI	0.23	76.47	100.00
	CMEMS INTERP	0.23	76.47	100.00
	CERTO OLCI	0.43	58.07	100.00
C	CMEMS OLCI	0.80	235.14	52.37
	CMEMS MULTI	0.62	173.27	84.10
	CMEMS INTERP	0.57	177.36	99.89
	CERTO OLCI	0.96	135.94	53.16
D	CMEMS OLCI	23.17	88.22	83.00
	CMEMS MULTI	8.68	52.40	93.38
	CMEMS INTERP	8.57	52.08	96.17
	CERTO OLCI	11.46	94.10	96.44

Table 4. Comparison of valid R_{rs} from different ocean color products in the Black Sea between 1 July 2016 and 30 June 2024. Rate of valid R_{rs} is calculated by dividing the number of valid R_{rs} by the number of days. "All bands" represents all available bands from each product, while "Six bands" represents the common six bands between CMEMS and CERTO products: 413 nm, 443 nm, 490 nm, 510 nm, 560 nm and 665 nm (note CERTO MSI only include four out of the six bands).

Band	Source	Satellite	*N* of days	*N* of R_{rs} matchup	*N* of valid R_{rs}	Rate of valid R_{rs} (%)
All bands	CMEMS	MULTI	2922	2043	2043	69.92
	CMEMS	OLCI	2922	1446	642	21.97
	CERTO	OLCI	2922	1732	236	8.08
	CERTO	MSI	2922	347	125	4.28
Six bands	CMEMS	MULTI	2922	2043	2043	69.92
	CMEMS	OLCI	2922	1446	1353	46.30
	CERTO	OLCI	2922	1732	1718	58.80
	CERTO	MSI	2922	347	347	11.88

phytoplankton light absorption characteristics in Chl-a maximum layer of the Black Sea (Churilova et al. 2019). However, none of them have used such a large and comprehensive *in situ* optical and biogeochemical dataset as compiled in our research. Knowing the most accurate ocean color products could support researchers in hydrological and climate modeling, and support water management sectors through the delineation of algal bloom or sediment plume area detections.

Although efforts have been made to ensure the quality of *in situ* data, potential uncertainties exist that might have influenced our validation work. First, the R_{rs} data were measured from different methods, which includes above-water and below-water approaches, and different platforms, including Profiler, TriOS, HyperSAS, and AERONET-OC. These measurements were made over different time periods and at different locations, mainly determined by instrument availability. The consistency between them has not been investigated in the present research, mainly because of the lack of concurrent measurements. In addition, some bands are not available from Profiler and AERONET-OC, making the number of matchups much lower than that of other bands (Figures 4–7). This led to the lack of comparable results between different bands for R_{rs} products. The band shifting method we used to convert the R_{rs} measured by Profiler and AERONET-OC to the OLCI, MSI, and MULTI bands potentially contributed some uncertainties but can be considered very limited because most (about 76%) of the wavelength differences were smaller than 3 nm. *In situ* Chl-a data were collected from two main approaches including HPLC and spectrophotometry. This introduces a certain degree of impact on uncertainty to the validation practice because of the recognized differing accuracy between these two methods. We did investigate their correlation using concurrent Chl-a data, which showed good consistency through a R^2 of 0.84 and an average difference of 0.11 mg/m^3, thus impacts to validation uncertainty are likely low. A follow-up analysis showed that using only HPLC-measured Chl-a for validations provided the same conclusions as found in Figure 8. In addition, we only considered Chl-a and TSM measured from the surface of the water in the Black Sea. Future work should focus on the inclusion of data from the water column. Propagating uncertainties from the *in situ* data into the ocean color product validations should also be considered in future studies.

4.2. Recommendations for improving the ocean color products

Our analysis suggested that R_{rs} products from both the CMEMS (MULTI and OLCI) and CERTO (OLCI and MSI) showed overall good accuracies in the visible bands (Figures 4–7), ensuring the correct input for algorithms that employ these bands. However, both products showed larger errors at short-blue bands (<440 nm) compared to visible bands, and most were overestimated. R_{rs} at NIR bands (>700 nm) also presented larger errors, with some underestimations for all four products. Particularly, we observed some negative values at short-blue and NIR bands in both the CMEMS and CERTO OLCI R_{rs} products (Figures 5 and 6), as well as the CERTO MSI product (Figure 7), which could impact ocean color applications. For instance, when considering Chl-a estimation for productive waters which employs 709 nm (e.g. Liu et al. 2021) and TSM estimation for high sediment waters, which employs 754 nm and 865 nm (e.g. Jiang et al. 2021b). Therefore, further developments are required to improve the accuracy of atmospheric correction methods, especially in the short-blue and NIR bands. The release of the new standard OLCI WFR product (collection 4) expected in early 2026 may bring improvements for the Black Sea ocean color products. Otherwise, the inclusion of ad-hoc atmospheric correction (e.g. POLYMER) in the operational processing chain should be considered.

As expected, Chl-a and TSM from CMEMS, EUMETSAT, and CERTO showed different accuracies across different OWTs since they are based on different atmospheric correction and retrieval algorithms. Blending algorithms used in different services could potentially improve the Chl-a and TSM estimates in the Black Sea. For instance, adding the Chl-a algorithm for turbid waters used in CERTO (Gitelson et al. 2011) to the current operational algorithm blending scheme for moderate and clear waters from CMEMS (Kajiyama, D'Alimonte, and Zibordi 2018), and a blend of the EUMETSAT TSM algorithm in turbid waters with the CERTO TSM algorithm in clear waters. Our results also emphasized the importance of regional calibrated algorithms. The above-mentioned findings that CMEMS OLCI performs better in low Chl-a waters while CERTO OLCI in high Chl-a waters, which is possibly because CMEMS Chl-a algorithm was calibrated with *in situ* data mainly from clear waters (<10 mg/m^3, Kajiyama, D'Alimonte, and Zibordi 2018), while CERTO Chl-a algorithm was calibrated with *in situ* Chl-a mostly from eutrophic waters in European transitional water systems including the Danube Delta. The OC4ME algorithm is also an empirical algorithm, but we found that it is not suitable for the Black Sea, as it was not developed specifically for these waters. Other researches also reported the same findings for the OC4 algorithm (Sancak et al. 2005; Suslin and Churilova 2016).

We also found spatial coverage differences between the CMEMS and CERTO OLCI products in our validation, which showed that CERTO provides a better coverage resulting in a higher number of valid matchups (Figures 5 and 6, Tables 3 and 4). The CERTO and CMEMS OLCI R_{rs} products are built on the same source imagery but using different atmospheric correction approaches: POLYMER + ACOLITE for CERTO and the standard OLCI WFR for CMEMS. Therefore, there are differences not only in terms of accuracy but also in terms of flagging, and it would be worthwhile to revisit the flagging approaches used in the processing chains.

5. Conclusions

A comprehensive *in situ* dataset was collected from the western, central, and eastern Black Seas to validate the accuracy of existing ocean color products provided by CMEMS, CERTO, and EUMETSAT in this area. We concluded that the R_{rs} products provided by both CMEMS and CERTO are accurate in the visible bands. However, further improvements are needed for R_{rs} in the short-blue (<440 nm) and NIR (>700 nm) bands. Chl-a and TSM from the CMEMS MULTI and OLCI, CERTO OLCI and MSI overall agree with *in situ*-measured values, but space exists for further improvements in specific water types for each of the products. The $K_d(490)$ products from the CMEMS provided accurate values across clear and turbid waters with a MAPD smaller than 20%.

Acknowledgements

The authors acknowledge the *in situ* data provided by the work done during the PhD project of A.M. Constantinescu, jointly funded by the University of Stirling (United Kingdom) and the National Institute of Marine Geology and GeoEcology—GeoEcoMar (Romania), ReCoReD (Reconstructing the Changing Impact of the Danube on the Black Sea

and Coastal Region), funded by TNA FP7 EuroFleets 2, Horizon 2020 Copernicus Evolution – Research for harmonized and Transitional water Observation (CERTO, No. 870349) project. We thank the General Bathymetric Chart of the Oceans (GEBCO) for the bathymetry and elevation data. For the AERONET radiometric products, we warmly acknowledge all principal investigators (Dr. Giuseppe Zibordi, Dr. Barbara Bulgarelli and Dr. Frederic Melin) for their efforts in establishing and maintaining of Gloria, Galata and Section-7 AERONET-OC sites in the western Black Sea. We thank Dr. G. Zibordi for his support with the AOP data processing and quality determination.

Author contributions

CRediT: **Dalin Jiang:** Conceptualization, Data curation, Formal analysis, Methodology, Writing – original draft; **Luis González Vilas:** Data curation, Investigation, Software, Writing – review & editing; **Elizabeth C. Atwood:** Data curation, Investigation, Software, Writing – review & editing; **Vittorio E. Brando:** Conceptualization, Investigation, Writing – review & editing; **Simone Colella:** Data curation, Software, Writing – review & editing; **Violeta Slabakova:** Data curation, Writing – review & editing; **Ivelin Petkov:** Data curation, Writing – review & editing; **Adriana Maria Constantinescu:** Data curation, Writing – review & editing; **Iulian Pojar:** Data curation, Writing – review & editing; **Adrian Stanica:** Conceptualization, Funding acquisition, Writing – review & editing; **Conor McGlinchey:** Data curation, Writing – review & editing; **Ximena Aguilar Vega:** Data curation, Writing – review & editing; **Douglas Moore:** Data curation, Writing – review & editing; **Evangelos Spyrakos:** Conceptualization, Investigation, Writing – review & editing; **Andrew Tyler:** Conceptualization, Funding acquisition, Writing – review & editing.

Disclosure statement

No potential conflict of interest was reported by the author(s).

Funding

This research was supported by the EU Horizon 2020 Developing Optimal and Open Research Support' for the Black Sea (DOORS, No. 101000518) project, the DANUBIUS Implementation Phase Project (DANUBIUS-IP 101079778), the Copernicus Marine Service Ocean Colour Thematic Assembly Center (21001L2-COP-TAC OC-2200 and 24251-COP TAC), and the UK Natural Environment Research Council's National Capability International project Future states Of the global Coastal ocean: Understanding for Solutions project (FOCUS, Ref. NE/X006271/1).

ORCID

Dalin Jiang 0000-0001-5676-5860

Data availability statement

Ocean color products evaluated in this research are openly available at CMEMS (https://marine.copernicus.eu), CERTO (https://engage.certo-project.org/data/) and EUMETSAT (https://www.eumetsat.int/ocean-colour-services). AERONET-OC *in situ* data are available at https://aeronet.gsfc.nasa.gov. The *in situ* Profiler multispectral reflectance and biogeochemical data from DOORS that support the findings of this study are openly available in Zenodo at https://doi.org/10.5281/zenodo.15173450 (Institute of Oceanology and Bulgarian Academy of Sciences (IO-BAS) 2025a), https://doi.org/10.5281/zenodo.15173206 (Institute of Oceanology and Bulgarian Academy of Sciences (IO-BAS) 2025b), https://doi.org/10.5281/zenodo.15259958 (Institute of Oceanology and Bulgarian Academy of Sciences (IO-BAS) 2025c); https://doi.org/10.5281/zenodo.14978829 (Institute of Oceanology and Bulgarian Academy of Sciences (IO-BAS) 2025 d); https://doi.org/10.5281/zenodo.15119521 (Institute of Oceanology and Bulgarian Academy of Sciences (IO-BAS) 2025e); https://doi.org/10.5281/zenodo.15120079 (Institute of Oceanology, Bulgarian Academy of Sciences (IO-BAS), 2025f). TriOS hyperspectral and HPLC Chl-a data from DOORS are openly available in Zenodo at https://doi.org/10.5281/zenodo.15778233 (Jiang et al. 2025c), https://doi.org/10.5281/zenodo.15778332 (Jiang et al. 2025d), https://doi.org/10.5281/zenodo.15778382 (Jiang et al. 2025e), with an embargo date until 31 May 2026. The other *in situ* data that support the findings of this study are available from the corresponding author, D. Jiang (dalin.jiang@stir.ac.uk), upon reasonable request.

References

Aronson, R. B., S. Thatje, J. B. McClintock, and K. A. Hughes. 2011. "Anthropogenic Impacts on Marine Ecosystems in Antarctica." *Annals of the New York Academy of Sciences* 1223 (1): 82–107. https://doi.org/10.1111/j.1749-6632.2010.05926.x.

Atwood, E. C., T. Jackson, A. Laurenson, B. F. Jönsson, E. Spyrakos, D. Jiang, S. Groom, et al. 2024. "Framework for Regional to Global Extension of Optical Water Types for Remote Sensing of Optically Complex Transitional Water Bodies." *Remote Sensing* 16 (17): 3267. https://doi.org/10.3390/rs16173267.

Aurin, D., A. Mannino, and D. J. Lary. 2018. "Remote Sensing of CDOM, CDOM Spectral Slope, and Dissolved Organic Carbon in the Global Ocean." *Applied Sciences* 8 (12): 2687. https://doi.org/10.3390/app8122687.

Barale, V., P. Cipollini, A. Davidov, and F. Melin. 2002. "Water Constituents in the North-Western Black Sea from Optical Remote Sensing and in Situ Data." *Estuarine, Coastal and Shelf Science* 54 (3): 309–320. https://doi.org/10.1006/ecss.2000.0649.

Barbier, E. B. 2017. "Marine Ecosystem Services." *Current Biology* 27 (11): R507–R510. https://doi.org/10.1016/j.cub.2017.03.020.

Brando, V. E., R. Santoleri, S. Colella, G. Volpe, A. Di Cicco, M. Sammartino, C. Lebreton, et al. 2024. "Overview of Operational Global and Regional Ocean Colour Essential Ocean Variables Within the Copernicus Marine Service." *Remote Sensing* 16 (23): 4588. https://doi.org/10.3390/rs16234588.

Churilova, T., V. Suslin, H. M. Sosik, T. Efimova, N. Moiseeva, S. Moncheva, O. Krivenko, V. Mukhanov, and O. Rylkova. 2019. "Phytoplankton Light Absorption in the Deep Chlorophyll Maximum Layer of the Black Sea." *European Journal of Remote Sensing* 52 (sup1): 123–136. https://doi.org/10.1080/22797254.2018.1533389.

Colella, S., Brando, V., Di Cicco, A., D'Alimonte, D., Forneris, V., and Bracaglia, M. 2025 Ocean Colour Mediterranean and Black Sea Observation Product https://documentation.marine.copernicus.eu/QUID/CMEMS-OC-QUID-009-141to144-151to154.pdf

Concha, J. A., M. Bracaglia, and V. E. Brando. 2021. "Assessing the Influence of Different Validation Protocols on Ocean Colour Match-Up Analyses." *Remote Sensing of Environment* 259: 112415. https://doi.org/10.1016/j.rse.2021.112415.

Constantin, S., D. Doxaran, and Ș. Constantinescu. 2016. "Estimation of Water Turbidity and Analysis of Its Spatio-Temporal Variability in the Danube River Plume (Black Sea) Using MODIS Satellite Data." *Continental shelf research* 112: 14–30. https://doi.org/10.1016/j.csr.2015.11.009.

Constantin, S., I. D. Șerban, D. Doxaran, and F. d'Ortenzio. 2024. "Regional Challenges Concerning Derivation of Suspended Particulate Matter Concentration and Water Turbidity from Water Reflectance. a Case Study in the Western Black Sea." *Estuarine, Coastal and Shelf Science* 305: 108871. https://doi.org/10.1016/j.ecss.2024.108871.

Constantinescu, A. M. 2019. *Reconstructing changes in sediment input from the Danube into the Black Sea*. United Kingdom: Ph.D. University of Stirling, Available at http://hdl.handle.net/1893/31886

Douville, H., K. Raghavan, J. Renwick, R. P. Allan, P. A. Arias, M. Barlow, and O. Zolina. 2021. Water Cycle Changes In *Climate Change 2021: The Physical Science Basis. Contribution of Working Group I to the Sixth Assessment Report of the Intergovernmental Panel on Climate Change*. Cambridge University Press.

Duarte, C. M. 2014. "Global Change and the Future Ocean: a Grand Challenge for Marine Sciences." *Frontiers in Marine Science* 1: 63. https://doi.org/10.3389/fmars.2014.00063.

EUMETSAT 2021. Sentinel-3 OLCI L2 report for baseline collection OL_L2M_003 - EUM/RSP/REP/21/1211386. Available at: (Accessed September 15, 2025) https://user.eumetsat.int/s3/eup-strapi-media/Sentinel_3_OLCI_L2_report_for_baseline_collection_OL_L2_M_003_2_B_c8bbc6d986.pdf

EUMETSAT 2022. Recommendations for sentinel-3 OLCI Ocean Colour product validations in comparison with in situ measurements – matchup protocols. Available at: (Accessed September 15, 2025) https://user.eumetsat.int/s3/eup-strapi-media/Recommendations_for_Sentinel_3_OLCI_Ocean_Colour_product_validations_in_comparison_with_in_situ_measurements_Matchup_Protocols_V8_B_e6c62ce677.pdf

Gitelson, A. A., B.-C. Gao, R.-R. Li, S. Berdnikov, and V. Saprygin. 2011. "Estimation of chlorophyll-a Concentration in Productive Turbid Waters Using a Hyperspectral Imager for the Coastal Ocean—the Azov Sea Case Study." *Environmental Research Letters* 6: 024023. https://doi.org/10.1088/1748-9326/6/2/024023.

Grégoire, M., A. Alvera-Azcaráte, L. Buga, A. Capet, S. Constantin, F. D'ortenzio, M. H. Rio, et al. 2023. "Monitoring Black Sea Environmental Changes from Space: New Products for Altimetry, Ocean Colour and Salinity. Potentialities and Requirements for a Dedicated In-Situ Observing System." *Frontiers in Marine Science* 9: 998970. https://doi.org/10.3389/fmars.2022.998970.

Groom, S., S. Sathyendranath, Y. Ban, S. Bernard, R. Brewin, V. Brotas, M. Wang, et al. 2019. "Satellite Ocean Colour: Current Status and Future Perspective." *Front Mar Sci* 6: 485. https://doi.org/10.3389/fmars.2019.00485.

Güttler, F. N., S. Niculescu, and F. Gohin. 2013. "Turbidity Retrieval and Monitoring of Danube Delta Waters Using Multi-Sensor Optical Remote Sensing Data: an Integrated View from the Delta Plain Lakes to the Western–northwestern Black Sea Coastal Zone." *Remote Sensing of Environment* 132: 86–101. https://doi.org/10.1016/j.rse.2013.01.009.

Hu, C., Z. Lee, and B. Franz. 2012. "Chlorophyll Algorithms for Oligotrophic Oceans: a Novel Approach Based on Three-Band Reflectance Difference." *Journal of Geophysical Research: Oceans* 117(C1): 1–25. https://doi.org/10.1029/2011JC007395.

Institute of Oceanology, Bulgarian Academy of Sciences (IO-BAS) 2025a Apparent Optical Properties DOORS cruise 1, 01-20 May, 2023 [Dataset]. Zenodo. https://doi.org/10.5281/zenodo.15173450.

Institute of Oceanology, Bulgarian Academy of Sciences (IO-BAS) 2025b Apparent Optical Properties DOORS cruise 2, leg 1, 01-10 September, 2023 [Dataset]. Zenodo. https://doi.org/10.5281/zenodo.15173206.

Institute of Oceanology, Bulgarian Academy of Sciences (IO-BAS) 2025c Apparent Optical Properties DOORS cruise 3, 01-20 June, 2024 [Dataset]. Zenodo. https://doi.org/10.5281/zenodo.15259958.

Institute of Oceanology, Bulgarian Academy of Sciences (IO-BAS) 2025d Chlorophyll a, Total Suspended Matter and Secchi Depth - DOORS 1 cruise, May 2023 [Dataset]. Zenodo. https://doi.org/10.5281/zenodo.14978829.
Institute of Oceanology, Bulgarian Academy of Sciences (IO-BAS) 2025e Chlorophyll a, Total Suspended Matter and Secchi Depth - DOORS 2 cruise, leg 1, September 2023 [Dataset]. Zenodo. https://doi.org/10.5281/zenodo.15119521.
Institute of Oceanology, Bulgarian Academy of Sciences (IO-BAS) 2025f Chlorophyll a, Total Suspended Matter and Secchi Depth - DOORS 3 cruise, June 2024 [Dataset]. Zenodo. https://doi.org/10.5281/zenodo.15120079.
Jackson, T., and Atwood, E. 2022 WP4 Optimal algorithms. CERTO deliverable D4.4. https://certo-project.org/Resources/D4.4_Optimal_algorithms_final.pdf
Jackson, T., S. Sathyendranath, and F. Mélin. 2017. "An Improved Optical Classification Scheme for the Ocean Colour Essential Climate Variable and Its Applications." *Remote Sensing of Environment* 203: 152–161. https://doi.org/10.1016/j.rse.2017.03.036.
Janelidze, N., E. Jaiani, N. Lashkhi, A. Tskhvediani, T. Kokashvili, T. Gvarishvili, M. Tediashvili, et al. 2011. "Microbial Water Quality of the Georgian Coastal Zone of the Black Sea." *Marine pollution bulletin* 62 (3): 573–580. https://doi.org/10.1016/j.marpolbul.2010.11.027.
Jeffrey, S. T., and G. F. Humphrey. 1975. "New Spectrophotometric Equations for Determining Chlorophylls A, B, c1 and c2 in Higher Plants, Algae and Natural Phytoplankton." *Biochemie und physiologie der pflanzen* 167 (2): 191–194. https://doi.org/10.1016/S0015-3796(17)30778-3.
Jiang, D., A. Marino, M. Ionescu, M. Gvilava, Z. Savaneli, C. Loureiro, A. Stanica, E. Spyrakos, and A. Tyler. 2025a. "Combining Optical and Sar Satellite Data to Monitor Coastline Changes in the Black Sea." *ISPRS Journal of Photogrammetry and Remote Sensing* 226: 102–115. https://doi.org/10.1016/j.isprsjprs.2025.05.003.
Jiang, D., Tyler, A., Hunter, P., Spyrakos, E., Riddick, C., Mascarenhas, V., Bresciani, M., Brito, A., Sent, G., Constantinescu, A., Vicente, V., Braga, F., Lebreton, C. 2021a) Gap analysis of standards and procedures and recommendations to IOCCG for bio-optical data acquisitionCopernicus Evolution–Research for harmonised and Transitional-water Observation (CERTO) deliverable D3.2 https://certo-project.org/getattachment/resources/CERTO_D3_2_Gap_analysis_of_bio-optical_protocols_FINAL.pdf?lang=en-GB
Jiang, D., B. Matsushita, and W. Yang. 2020. "A Simple and Effective Method for Removing Residual Reflected Skylight in Above-Water Remote Sensing Reflectance Measurements." *ISPRS Journal of Photogrammetry and Remote Sensing* 165: 16–27. https://doi.org/10.1016/j.isprsjprs.2020.05.003.
Jiang, D., B. Matsushita, F. Setiawan, and A. Vundo. 2019. "An Improved Algorithm for Estimating the Secchi Disk Depth from Remote Sensing Data Based on the New Underwater Visibility Theory." *ISPRS journal of photogrammetry and remote sensing* 152: 13–23. https://doi.org/10.1016/j.isprsjprs.2019.04.002.
Jiang, D., B. Matsushita, N. Pahlevan, D. Gurlin, M. K. Lehmann, C. G. Fichot, D. O'Donnell, et al. 2021b. "Remotely Estimating Total Suspended Solids Concentration in Clear to Extremely Turbid Waters Using a Novel Semi-Analytical Method." *Remote sensing of environment* 258: 112386. https://doi.org/10.1016/j.rse.2021.112386.
Jiang, D., B. Matsushita, N. Pahlevan, D. Gurlin, C. G. Fichot, J. Harringmeyer, E. Spyrakos, et al. 2023. "Estimating the Concentration of Total Suspended Solids in Inland and Coastal Waters from Sentinel-2 MSI: a Semi-Analytical Approach." *ISPRS Journal of Photogrammetry and Remote Sensing* 204: 362–377. https://doi.org/10.1016/j.isprsjprs.2023.09.020.
Jiang, D., McGlinchey, C., Slabakova, V., Petkov, I., Shaw, D., Spyrakos, E., and Tyler, A. 2025c Optical and biogeochemical data from DOORS cruise 1, 01-20 May 2023 (1.0) [Dataset]. Zenodo. https://doi.org/10.5281/zenodo.15778233.
Jiang, D., Slabakova, V., Petkov, I., Spyrakos, E., and Tyler, A. 2025e Optical and biogeochemical data from DOORS cruise 3, 01-20 June 2024 (1.0) [Dataset]. Zenodo. https://doi.org/10.5281/zenodo.15778382
Jiang, D., Aguilar Vega, X., Slabakova, V., Petkov, I., Moore, D., Spyrakos, E., and Tyler, A 2025d Optical and biogeochemical data from DOORS cruise 2, 01-10 September 2023 (1.0) [Dataset]. Zenodo. https://doi.org/10.5281/zenodo.15778332.
Jiang, D., V. Khokhlov, Y. Tuchkovenko, D. Kushnir, V. Ovcharuk, E. Spyrakos, A. Tyler, A. Stanica, and V. Slabakova. 2025b. "The Biogeochemical Response of the North-Western Black Sea to the Kakhovka Dam Breach." *Communications Earth & Environment* 6 (1): 185. https://doi.org/10.1038/s43247-025-02153-z.
Kajiyama, T., D. D'Alimonte, and G. Zibordi. 2018. "Algorithms Merging for the Determination of chlorophyll-a Concentration in the Black Sea." *IEEE Geoscience and Remote Sensing Letters* 16 (5): 677–681. https://doi.org/10.1109/LGRS.2018.2883539.
Kideys, A. E. 2002. "Fall and Rise of the Black Sea Ecosystem." *Science* 297: 1482–1484. https://doi.org/10.1126/science.1073002.
Kopelevich, O., V. Burenkov, S. Sheberstov, S. Vazyulya, M. Kravchishina, L. Pautova, A. Grigoriev, V. Silkin, and V. Artemiev. 2014. "Satellite Monitoring of Coccolithophore Blooms in the Black Sea from Ocean Color Data." *Remote sensing of environment* 146: 113–123. https://doi.org/10.1016/j.rse.2013.09.009.
Kukushkin, A. S., and V. V. Suslin. 2020. "Assessment of Applicability of Satellite-Derived Ocean Color Data for Studying Variability of Total Suspended Matter in the Surface Layer of the Deep Part of the Black Sea." *Physical Oceanography* 27 (5): 547–556. https://doi.org/10.22449/1573-160X-2020-5-547-556.
Lee, Z., S. Shang, C. Hu, K. Du, A. Weidemann, W. Hou, J. Lin, G. Lin. 2015. "Secchi Disk Depth: a New Theory and Mechanistic Model for Underwater Visibility." *Remote sensing of environment* 169: 139–149. https://doi.org/10.1016/j.rse.2015.08.002.

Lin, J., Atwood, E. C., Liu, X., Nwokocha, E., Jackson, T., and Groom, S. 2026. Improved Suspended Particulate Matter estimation using algorithm selection based on Optical Water Types for transitional water systems. (submitted).
Liquete, C., C. Piroddi, E. G. Drakou, L. Gurney, S. Katsanevakis, A. Charef, and B. Egoh. 2013. "Current Status and Future Prospects for the Assessment of Marine and Coastal Ecosystem Services: a Systematic Review." *PLoS One* 8 (7): e67737. https://doi.org/10.1371/journal.pone.0067737.
Liu, X., C. Steele, S. Simis, M. Warren, A. Tyler, E. Spyrakos, P. Hunter, and N. Selmes. 2021. "Retrieval of Chlorophyll-a Concentration and Associated Product Uncertainty in Optically Diverse Lakes and Reservoirs." *Remote Sensing of Environment* 267: 112710. https://doi.org/10.1016/j.rse.2021.112710.
Mélin, F., and G. Sclep. 2015. "Band Shifting for Ocean Color Multi-Spectral Reflectance Data." *Optics Express* 23 (3): 2262–2279. https://doi.org/10.1364/OE.23.002262.
Moore, T. S., J. W. Campbell, and H. Feng. 2001. "A Fuzzy Logic Classification Scheme for Selecting and Blending Satellite Ocean Color Algorithms." *IEEE Transactions on Geoscience and Remote Sensing : A Publication of the IEEE Geoscience and Remote Sensing Society* 39: 1764–1776. https://doi.org/10.1109/36.942555.
Morel, A., Y. Huot, B. Gentili, P. J. Werdell, S. B. Hooker, and B. A. Franz. 2007. "Examining the Consistency of Products Derived from Various Ocean Color Sensors in Open Ocean (Case 1) Waters in the Perspective of a Multi-Sensor Approach." *Remote Sensing of Environment* 111 (1): 69–88. https://doi.org/10.1016/j.rse.2007.03.012.
Murray, J. W., Z. Top, and E. Özsoy. 1991. "Hydrographic Properties and Ventilation of the Black Sea." *Deep Sea Res. Part A Oceanogr. Res. Pap.* 38: S663–S689. https://doi.org/10.1016/S0198-0149(10)80003-2.
Nazirova, K., Y. Alferyeva, O. Lavrova, Y. Shur, D. Soloviev, T. Bocharova, and A. Strochkov. 2021. "Comparison of in Situ and Remote-Sensing Methods to Determine Turbidity and Concentration of Suspended Matter in the Estuary Zone of the Mzymta River, Black Sea." *Remote Sensing* 13 (1): 143. https://doi.org/10.3390/rs13010143.
Nechad, B., K. G. Ruddick, and Y. Park. 2010. "Calibration and Validation of a Generic Multisensor Algorithm for Mapping of Total Suspended Matter in Turbid Waters." *Remote Sensing of Environment* 114 (4): 854–866. https://doi.org/10.1016/j.rse.2009.11.022.
O'Reilly, J. E., and P. J. Werdell. 2019. "Chlorophyll Algorithms for Ocean Color sensors-OC4, OC5 & Oc6." *Remote sensing of environment* 229: 32–47. https://doi.org/10.1016/j.rse.2019.04.021.
Sancak, S., S. T. Besiktepe, A. Yilmaz, M. Lee, and R. Frouin. 2005. "Evaluation of SeaWiFS chlorophyll-a in the Black and Mediterranean Seas." *International Journal of Remote Sensing* 26 (10): 2045–2060. https://doi.org/10.1080/01431160512331337853.
Shanmugam, P. 2011. "New Models for Retrieving and Partitioning the Colored Dissolved Organic Matter in the Global Ocean: Implications for Remote Sensing." *Remote sensing of Environment* 115 (6): 1501–1521. https://doi.org/10.1016/j.rse.2011.02.009.
Steinmetz, F., and Ramon, D. 2023 Final product evaluation and description of algorithmic evolutionsCERTO deliverable D5.4 https://certo-project.org/Resources/CERTO_D5.4_final.pdf
Steinmetz, F., P. Y. Deschamps, and D. Ramon. 2011. "Atmospheric Correction in Presence of Sun Glint: Application to Meris." *Optics express* 19 (10): 9783–9800. https://doi.org/10.1364/OE.19.009783.
Stramski, D., I. Joshi, and R. A. Reynolds. 2022. "Ocean Color Algorithms to Estimate the Concentration of Particulate Organic Carbon in Surface Waters of the Global Ocean in Support of a Long-Term Data Record from Multiple Satellite Missions." *Remote Sensing of Environment* 269: 112776. https://doi.org/10.1016/j.rse.2021.112776.
Suslin, V., and T. Churilova. 2016. "A Regional Algorithm for Separating Light Absorption By chlorophyll-a and Coloured Detrital Matter in the Black Sea, Using 480–560 Nm Bands from Ocean Colour Scanners." *International Journal of Remote Sensing* 37 (18): 4380–4400. https://doi.org/10.1080/01431161.2016.1211350.
Van der Zande, D., Stelzer, K., Lebreton, C., Dille, A., Shevchuk, R., Santos, J., Böttcher, M., Vanhellemont, Q., Scholze, J. 2024) High resolution Ocean Colour Product https://documentation.marine.copernicus.eu/QUID/CMEMS-HR-OC-QUID-009-201to212.pdf
Vanhellemont, Q., and K. Ruddick. 2018. "Atmospheric Correction of Metre-Scale Optical Satellite Data for Inland and Coastal Water Applications." *Remote sensing of environment* 216: 586–597. https://doi.org/10.1016/j.rse.2018.07.015.
Vespremeanu, E. and M. Golumbeanu. 2017. *The Black Sea: Physical, Environmental and Historical Perspectives*. Springer.
Volpe, G., B. B. Nardelli, S. Colella, A. Pisano, and R. Santoleri. 2018. "An Operational Interpolated Ocean Colour Product in the Mediterranean Sea." *New Frontiers in Operational Oceanography*. 227–244.
Vostokov, S. V., A. S. Vostokova, and S. V. Vazyulya. 2022. "Seasonal and Long-Term Variability of Coccolithophores in the Black Sea According to Remote Sensing Data and the Results of Field Investigations." *Journal of Marine Science and Engineering* 10 (1): 97. https://doi.org/10.3390/jmse10010097.
Wang, S., J. Li, B. Zhang, Z. Lee, E. Spyrakos, L. Feng, X. Zhang, et al. 2020. "Changes of Water Clarity in Large Lakes and Reservoirs Across China Observed from Long-Term Modis." *Remote Sensing of Environment* 247: 111949. https://doi.org/10.1016/j.rse.2020.111949.
Warren, M. A., S. G. Simis, V. Martinez-Vicente, K. Poser, M. Bresciani, K. Alikas, A. Ansper, E. Spyrakos, and C. Giardino. 2019. "Assessment of Atmospheric Correction Algorithms for the Sentinel-2A MultiSpectral Imager over Coastal and Inland Waters." *Remote sensing of environment* 225: 267–289. https://doi.org/10.1016/j.rse.2019.03.018.
Wegwerth, A., B. Plessen, I. C. Kleinhanns, and H. W. Arz. 2021. "Black Sea Hydroclimate and Coupled Hydrology Was Strongly Controlled By High-Latitude Glacial Climate Dynamics." *Commun. Earth Environ.* 2: 63. https://doi.org/10.1038/s43247-021-00129-3.

Wilson, H., N. Raasakka, E. Spyrakos, D. Millar, M. B. Neely, A. Salyani, A. Tyler, et al. 2025. "Unlocking the Global Benefits of Earth Observation to Address the SDG 6 in Situ Water Quality Monitoring Gap." *Frontiers in Remote Sensing* 6: 1549286. https://doi.org/10.3389/frsen.2025.1549286.

Yunev, O. A., J. Carstensen, L. V. Stelmakh, V. N. Belokopytov, and V. V. Suslin. 2021. "Reconsideration of the Phytoplankton Seasonality in the Open Black Sea." *Limnology and Oceanography Letters* 6 (1): 51–59. https://doi.org/10.1002/lol2.10178.

Zibordi, G., B. N. Holben, M. Talone, D. D'Alimonte, I. Slutsker, D. M. Giles, and M. G. Sorokin. 2021. "Advances in the Ocean Color Component of the Aerosol Robotic Network (Aeronet-Oc)." *Journal of Atmospheric and Oceanic Technology* 38 (4): 725–746. https://doi.org/10.1175/JTECH-D-20-0085.1.

Zibordi, G., E. Kwiatkowska, F. Mélin, M. Talone, I. Cazzaniga, D. Dessailly, and J. I. Gossn. 2022. "Assessment of OLCI-A and OLCI-B Radiometric Data Products Across European Seas." *Remote Sensing of Environment* 272: 112911. https://doi.org/10.1016/j.rse.2022.112911.

Zibordi, G., F. Mélin, and J.-F. Berthon. 2018. "A Regional Assessment of OLCI Data Products." *IEEE Geoscience and Remote Sensing Letters* 15: 1490–1494. https://doi.org/10.1109/LGRS.2018.2849329.

Zibordi, G., J.-F. Berthon, F. Mélin, and D. D'Alimonte. 2011. "Cross-Site Consistent in Situ Measurements for Satellite Ocean Color Applications: the BiOMaP Radiometric Dataset." *Remote Sensing of Environment* 115: 2104–2115. https://doi.org/10.1016/j.rse.2011.04.013.